Bioconjugate Chemistry

Article

pubs.acs.org/bc

pH-Triggered Nanoparticle Mediated Delivery of siRNA to Liver Cells in Vitro and in Vivo

Soumia Kolli,[†] Suet-Ping Wong,[‡] Richard Harbottle,[‡] Brian Johnston,[§] Maya Thanou,[∥] and Andrew D. Miller*[,†,∥]

[†]Imperial College Genetic Therapies Centre, Department of Chemistry, Flowers Building, Armstrong Road, Imperial College London, London SW7 2AZ, United Kingdom

[‡]Gene Therapy Research Group, Section of Molecular and Cellular Medicine, National Heart and Lung Institute, Imperial College London, London, SW7 2AZ, United Kingdom

[§]Somagenics, 2161 Delaware Avenue, Santa Cruz, California 95060, United States

[∥]Institute of Pharmaceutical Science, Kings College London, Franklin-Wilkins Building, Waterloo Campus, 150 Stamford Street, London SE1 9NH, United Kingdom

Supporting Information

ABSTRACT: Recently, we reported for the first time the development of pH-triggered nanoparticles for the functional delivery of small interfering RNA (siRNA) to liver for treatment of hepatitis B virus infections in vivo. Here, we report on systematic formulation and biophysical studies of three different pH-triggered nanoparticle formulations looking for ways to improve on the capabilities of our previous nanoparticle system. We demonstrate how pH-triggered, PEGylated siRNA nanoparticles stable with respect to aggregation in 80% serum can still release siRNA payload at pH 5.5 within 30 min. This capability allows functional delivery to cultured murine hepatocyte cells in vitro, despite a high degree of PEGylation (5 mol %). We also demonstrate that pH-triggered, PEGylated siRNA nanoparticles typically enter cells by clathrin-coated pit endocytosis, but functional delivery requires membrane fusion events (fusogenicity). Biodistribution studies indicate that >70% of our administered nanoparticles are found in liver hepatocytes, post intravenous administration. Pharmacodynamic experiments show siRNA delivery to murine liver effecting maximum knockdown 48 h post administration from a single dose, while control (nontriggered) nanoparticles require 96 h and two doses to demonstrate the same effect. We also describe an anti-hepatitis C virus (HCV) proof-of-concept experiment indicating the possibility of RNAi therapy for HCV infections using pH-triggered, PEGylated siRNA nanoparticles.

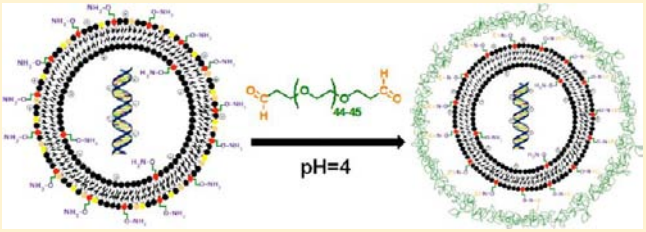

INTRODUCTION

The potential of RNA interference (RNAi) for therapy is well-known. So too is the need for vector delivery technologies that ensure efficient, functional delivery of RNAi effectors to target cells of interest in vivo.[1−3] Since 2002, a substantial number of different vector delivery technologies have been under investigation. Potentially useful technologies include the use of lipid-, peptide-, or antibody-based bioconjugates,[4,5] polyethylenimine (PEI) polymer-based systems for the delivery of RNAi effectors to tumors,[6,7] and biopolymer-based delivery systems such as those involving atelocollagen or chitosan.[8] On the other hand, there has been substantial industrial focus on lipid-based nanoparticles or corresponding lipidoid-based nanoparticle systems.[9−12]

Recently, we described three contrasting lipid-based nanoparticle systems for systemic delivery of small interfering RNAs (siRNAs) in vivo. The first involved just the use of a simple cationic lipid *N*′,*N*′-dioctadecyl-*N*-4,8-diaza-10-aminodecanoylglycine amide (DODAG) **1** (Figure 1) that assisted the functional delivery of anti-hepatitis B virus (HBV) siRNAs to liver in vivo, leading to a partial correction in the level of HBV infection in a murine model of this human disease.[13] The second comprised putative pH-triggered PEGylated siRNA nanoparticles (pH-triggered siRNA-**ABC** nanoparticles), that mediated more reliable and extended suppression of HBV infection levels in this same HBV infection model.[14] Finally, we described theranostic siRNA-**ABC** nanoparticles (labeled with MRI contrast agents and fluorescent probes) that effected functional delivery of anticancer siRNAs to tumors in vivo, causing siRNA-mediated phenotypic reductions in tumor growth with simultaneous diagnostic/real-time imaging of vector biodistribution and siRNA pharmacokinetics.[15]

The **ABC** nanoparticle terminology used above derives from the **ABCD** nanoparticle that was invoked previously as a means to define the structures of synthetic nanoparticles designed for the successful functional delivery of therapeutic nucleic acids in

Received: July 25, 2012
Revised: December 19, 2012
Published: January 10, 2013

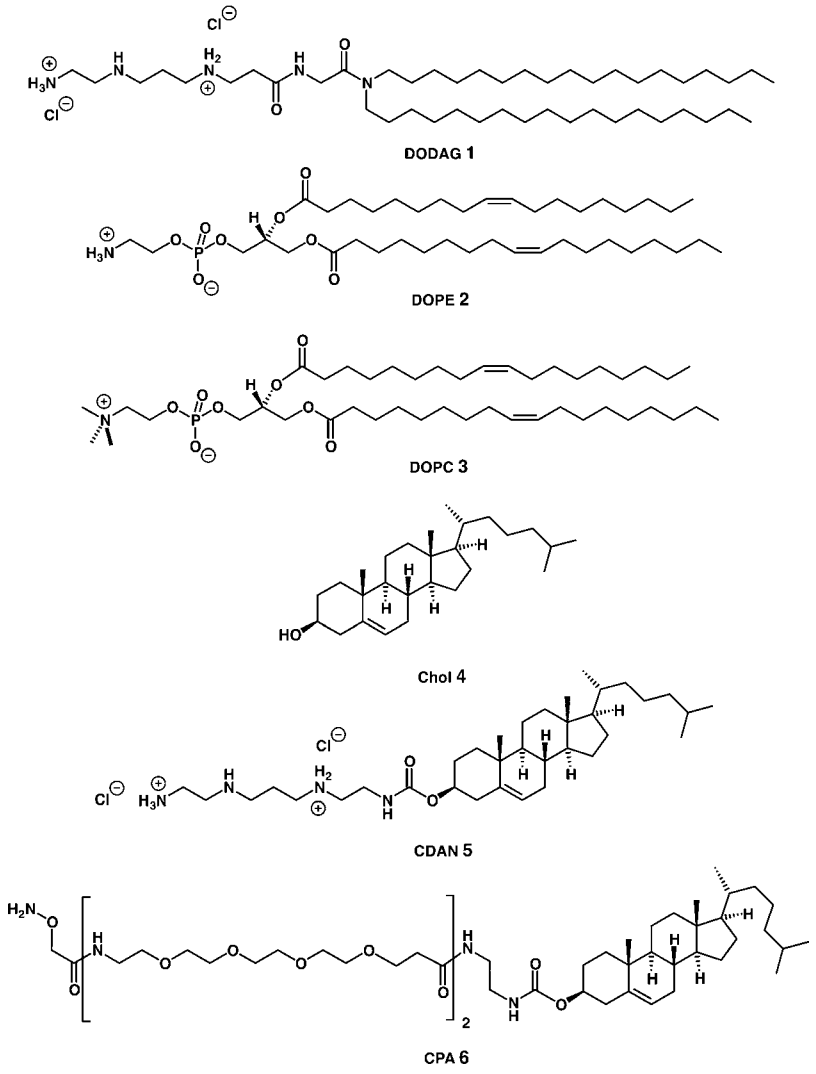

Figure 1. Summary of lipid structures used in the present investigations.

vivo (Scheme 1).[16] According to this general paradigm, functional nanoparticles comprise active pharmaceutical ingredients (**A**-component—RNAi effectors in our case here) surrounded initially by compaction/association agents (**B**-components—typically lipids, amphiphiles, proteins, or even synthetic polymers) designed to help sequester, carry, and promote functional delivery of the **A**-component. Such **AB**-core nanoparticles are considered to have some utility in vivo but more typically require coating with a stealth/biocompatibility polymer layer (**C**-component—most often polyethylene glycol [PEG]) designed to render resulting **ABC** nanoparticles with colloidal stability in biological fluids and immunoprotection from the reticuloendothelial system (RES) plus other immune system responses. Finally, an optional biological targeting layer (**D**-components—bona fide biological receptor specific ligands) might be added to confer the resulting **ABCD** nanoparticle with target cell specificity.

Importantly, experience has shown that the general **ABCD** nanoparticle paradigm itself has one primary design weakness in that the stealth biocompatibility polymer layer (typically PEG-based) (**C**-layer) does not prevent nanoparticle entry into cells but may substantially inhibit functional intracellular delivery of the active pharmaceutical ingredient, unless sufficiently removed by the time of target cell-entry or else during the process of cell-entry. Accordingly, in consideration of next steps toward improved nanoparticle delivery systems for

Scheme 1. Illustrations of siRNA-ABCD Nanoparticles Self-Assembled from Tool Kits of Chemical Components[a]

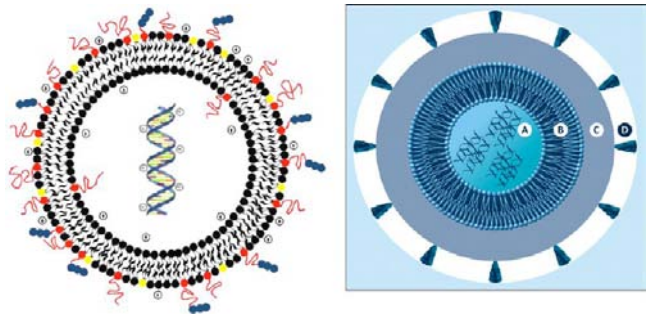

[a](Left) diagrammatic illustration showing the involvement of cationic lipids (black), helper lipids (yellow), PEGylated lipids (red), and targeting ligands (blue). (Right) schematic to show how nanoparticle core consists of siRNA (A-component) and lipid (B-components) stabilized by polymer coating (typically polyethylene glycol [PEG]; C-component) that also reduces interactions with the immune system. Optional targeting ligands (D-component) can be present to promote functional delivery of siRNA at the target cells of interest.

dx.doi.org/10.1021/bc3004099 | *Bioconjugate Chem.* 2013, 24, 314−332

RNAi effectors and other therapeutic nucleic acids such as plasmid DNA (pDNA), we have become increasingly interested in research leading to nanoparticles that possess the property of triggerability. Such nanoparticles are designed for high levels of stability in biological fluid from points of administration to target cells whereupon they become triggered for the controlled release of therapeutic agent payload(s) by changes in local endogenous conditions or through the application of an external/exogenous stimulus.[16,17]

In this respect, we recently described a new lipid-based nanoparticle system and a new polymer-based nanoparticle system, this time for the functional delivery of pDNA to murine lung. The lipid-based nanoparticle system was set up as a half-life-triggered nanoparticle system and the polymer-based nanoparticle as a redox-triggered nanoparticle system.[18,19] Experience gained from working with these triggered pDNA delivery systems and the pH-triggered nanoparticle system described above strongly suggested that triggerability should be a key characteristic of next generations of delivery nanoparticle technologies for the functional delivery of siRNA, pDNA and other nucleic acids in vivo with improved pharmacodynamics and potentially better clinical use prospects.

In recognition of this, we decided to make a more detailed study of our prototype pH-triggered nanoparticle system,[14] in the expectation of understanding this system better and of preparing the ground for the development of next generations of triggerable nanoparticle delivery systems. Here, we now report results from a systematic ground-up investigation into three separate pH-triggered siRNA-**ABC** nanoparticle formulations. This investigation culminates in a proof-of-concept demonstration for an RNAi therapeutic approach to hepatitis C virus (HCV) infection involving nanoparticle-mediated delivery of anti-HCV RNAi effectors to murine liver in vivo.

EXPERIMENTAL SECTION

General Experimental. Chemicals including lipids dioleoyl-L-α-phosphatidylethanolamine (DOPE) **2**, dioleoyl-L-α-phosphatidylcholine (DOPC) **3**, and cholesterol (Chol) **4** (Figure 1) were purchased from Sigma-Aldrich, Lancaster or Merck Biosciences. DODAG **1** was prepared as described previously,[13] as was N^1-cholesteryloxycarbonyl-3,7-diazanonane-1,9-diamine (CDAN) **5** (Figure 1).[20−22] The synthesis of cholesteryl PEG^{350} aminoxy (CPA) lipid **6** is described below and is a substantial variation on the previous published described solid-phase methodology (Figure 1; Scheme 2).[14] Unless otherwise stated, all reactions were carried out under an atmosphere of nitrogen or argon, in oven-dried glassware. CH_2Cl_2 was distilled over P_2O_5, while other solvents were bought and predried as required.

Flash column chromatography (Merck Kieselgel 60 F_{254} 230−240 mesh) was performed according to the method of Still et al.[23] Thin layer chromatography (TLC) was performed on precoated Merck silica gel (0.2 mm, 60 F_{254}) aluminum-backed plates, and visualized with a UV lamp (254 nm) and/or stained with acidic ammonium molybdate (IV), basic potassium manganate (VII), iodine, or phosphomolybdic acid. Chromatography solvent mixture A is as follows: CH_2Cl_2/MeOH/H_2O at 65:25:4 v/v/v).

HPLC was performed using Vydac C-4 reversed phase preparative column with 1 mL min^{-1} flow rate: mobile phases as follows used trifluoroacetic acid (TFA); **A**: H_2O (0.1% TFA); **B**: MeCN (0.1% TFA); **C**: MeOH (0.1% TFA).

Scheme 2. Synthesis of Cholesteryl PEG^{350}-aminoxy (CPA) Lipid[a]

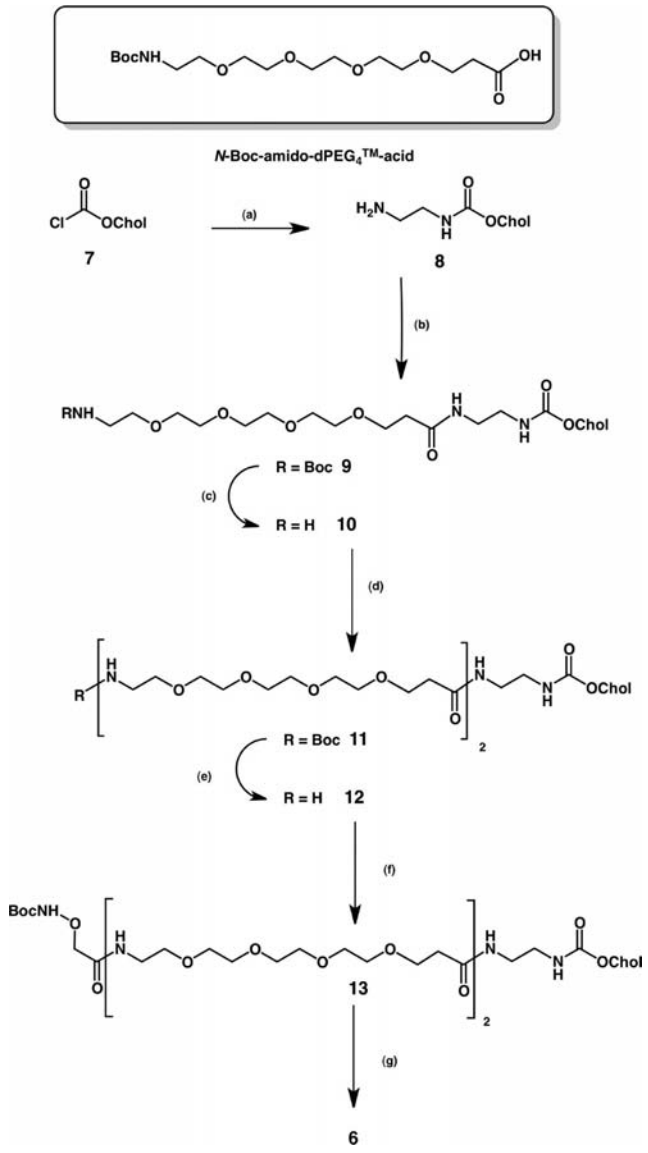

[a](a) Ethylene-1,2-diamine (solvent), 18 h, 73%; (b) *N*-Boc-amido-dPEG$_4$-acid (1 equiv.), HBTU (1.5 equiv) DMAP (3 equiv) in CH_2Cl_2, 24 h, 93%; (c) 50% (v/v) TFA in CH_2Cl_2, 2 h, 83%; (d) *N*-Boc-amido-dPEG$_4$-acid (1 equiv), HBTU (1.5 equiv), DMAP (3 equiv) in CH_2Cl_2, 24 h, 90%; (e) 50% (v/v) TFA in CH_2Cl_2, 2 h, 95%; (f) *N*-Boc-aminoxyacetic acid (1 equiv), HBTU (1.5 equiv), DMAP (3 equiv) in CH_2Cl_2, 24 h, 43%; (g) 4 M HCl, dioxane/propan-2-ol, 2 h, 73%.

Program set to 0−15.0 min (100%, **A**), 15.1−25.0 min (0−100%, **B**), 25.1−45 min (100%, **C**), 45.1−55 min (100%, **A**).

Melting points were measured on a Stuart Scientific SMP3 apparatus and are reported without correction.

Infrared spectra (IR) were measured on a JASCO FT/IR-620 spectrometer.

^{1}H NMR and ^{13}C NMR spectra were recorded on Bruker Avance 400 using residual isotopic solvent as a reference: ^{1}H NMR, (400 MHz) $CDCl_3$ δ_H = 7.27 ppm, CD_3OD δ_H = 3.30 ppm; ^{13}C NMR (100 MHz) $CDCl_3$ δ_C = 77.00 ppm, CD_3OD δ_C = 49.05 ppm. Peaks split by the presence of a phosphorus atom are indicated with a superscript p.

dx.doi.org/10.1021/bc3004099 | *Bioconjugate Chem.* 2013, 24, 314−332

Mass spectra were recorded using VG Platform II, VG-070B, Joel SX-102, or Bruker Esquire 3000 ESI instruments.

Elemental analysis was carried out using a Perkin-Elmer 2400 CHN elemental analyzer at the Science Technical Support unit, London Metropolitan University.

N^1-Cholesteryloxycarbonyl-1,2-diamine (Cholesterylamine) 8. Cholesteryl chloroformate **7** (7.5 g, 16.7 mmol) was dissolved in ethylene-1,2-diamine (180 mL) and the mixture stirred for 18 h. The reaction mixture was then quenched with water and extracted with CH_2Cl_2. The organic extracts were dried ($MgSO_4$) and the solvent was removed in vacuo to afford a residue, which was purified by flash column chromatography [CH_2Cl_2/MeOH/NH_3 at 192:7:1 to 92:7:1 (v/v/v)] giving purified **8** (5.5 g, 11.6 mmol, 73%) as a white solid (mp 175−177 °C): FTIR (Nujol mull) ν_{max} 3338 (amine), 2977 (alkane), 2830 (alkane), 1692 (carbamate) cm^{-1}; ^1H NMR (400 MHz, $CDCl_3$) δ_H 0.66 (3H, s, H-18), 0.846 (3H, d, J = 6.4 Hz, H-27), 0.850 (3H, d, J = 6.4 Hz, H-26), 0.898 (3H, d, J = 6.4 Hz, H-21), 0.922 (3H, s, H-19), 1.02−1.63 (21H, m, H-1, H-9, H-11, H-12, H-14, H-15, H-16, H-17, H-20, H-22, H-23, H-24, H-25), 1.76−2.1 (5H, m, H-2, H-7, H-8), 2.22−2.36 (2H, m, H-4), 2.79−2.81 (2H, m, $H_2NC\underline{H}_2$), 3.197−3.210 (2H, m, $H_2NCH_2C\underline{H}_2$), 4.52 (1H, m, H-3), 5.31 (1H, s, H-6); MS (ESI +ve) 473 (M + H); HRMS (FAB +ve) calculated for $C_{30}H_{53}N_2O_2$ (M + H) 473.4119, found 473.4107.

N^2-[N'^{15}-*t*Butyloxycarbonyl-(4,7,10,13-tetraoxa-15-aminopentadecanoyl)]-N^1-cholesteryloxycarbonyl-ethylene-1,2-diamine 9. N^{15}-*t*Butyloxycarbonyl-4,7,10,13-tetraoxa-15-aminopentadecanoic acid (0.600 g, 1.64 mmol, 1 equiv) and the cholesterylamine **8** (0.776 g, 1.64 mmol, 1 equiv) were dissolved in dry CH_2Cl_2 (7 mL) under nitrogen. Dimethylaminopyridine (DMAP) (0.601 g, 4.98 mmol, 3 equiv) and 2-(1*H*-benzotriazole-1-yl)-1,1,3,3-tetramethyluronium hexafluorophosphate (HBTU) (0.934 g, 0.319 mmol, and 1.5 equiv) were added to the solution. The reaction mixture stirred at room temperature under nitrogen for 24 h. The solution was diluted with CH_2Cl_2 (7 mL) washed successively with citric acid 7% aq solution and brine before being dried on Na_2SO_4. After removal of the solvent, the residue was purified by flash chromatography on silica column using CH_2Cl_2/MeOH/H_2O (at 78:9:1 v/v/v) to afford purified **9** as colorless oil that crystallized slowly (1.25 g, 1.52 mmol, yield 93%). R_f [CH_2Cl_2/MeOH/H_2O at 34.5:9:1 v/v/v] 0.43; FTIR: ν_{max} (nujol)/cm^{-1} 3656−3132, 2937, 2872, 1703, 1654, 1531, 1468, 1365, 1253, 1172, 1117. ^1H NMR (400 MHz, $CDCl_3$) δ_H 0.68 (3H, s, Chol H-18), 0.86, 0.88 (6H, 2d, J = 6.4 and 1.2 Hz), 0.92 (3H, d, J = 6.4 Hz, Chol H-21), 1.01 (3H, s, Chol H-19), 1.45 (9H, s, 3×C$\underline{H}_3$), 0.96−2.05 (Chol H-1, 2, 4, 7, 8, 9, 11, 12, 14, 15, 16, 17, 20, 22, 23, 25), 2.25−2.41 (2H, m, Chol H-24), 2.15 (m, NHCOC$\underline{H}_2$), 3.3 (4H, t, J = 5.2 Hz, 2×C$\underline{H}_2$), 3.5 (2H, m, C$\underline{H}_2$), 3.55 (2H, t, J = 5.2 Hz, C$\underline{H}_2$), 3.57−3.70 (6H, m, 3×C$\underline{H}_2$), 3.75 (2H, t, J = 5.2 Hz, C$\underline{H}_2$), 4.35 (s br, 1H, NH), 4.49 (1H, m, Chol H-3), 5.3 (1H, s br, N−H), 5.37 (1H, m, Chol H-6), 6.80 (1H, s br, N−H).^{13}C NMR (100 MHz, $CDCl_3$) δ_C = 11.68 (C-18), 18.54 (C-21), 19.15 (C-19), 20.86 (C-11), 22.38 (C-27), 22.64 (C-26), 23.64 (C-23), 24.09 (C-15), 27.80 (C-25), 28.03 (C-2 and C16), 28.26 (3×CH_3), 31.68 (C-8), 31.71 (C-7), 35.59 (C-20), 36.00 (C-22), 36.37 (C-10), 36.37 (C$\underline{H}_2$), 36.82 (C-1), 38.44 (C-24), 39.33 (C-12), 39.42 (NHC$\underline{H}_2$CH$_2$NH), 39.55 (C-4), 40.18 (NHC$\underline{H}_2$CH$_2$NH), 40.72 (C$\underline{H}_2$NHBoc), 42.12 (C-13), 49.84 (C-9), 55.96 (C-17), 56.51 (C-14), 67.11 (C$\underline{H}_2$O), 69.99−70.38 (7×C$\underline{H}_2$), 74.05 (C-3), 78.94 (C quat.), 122.26 (C-6), 139.64 (C-5), 155.89 (OCONH), 156.43 (OCONH), 172.10 (NH(C$\underline{O}$)CH$_2$); m/z (FAB + ve) [M+Na] 843. FAB-MS calculated for $C_{46}H_{82}N_3O_9$ [M+H] 820.6051, found 820.6069.

N^2-4,7,10,13-Tetraoxa-15-aminopentadecanoyl-N^1-cholesteryloxycarbonyl-ethylene-1,2-diamine 10. Amine protected compound **9** (1.2 g, 1.46 mmol) was dissolved in 10 mL of a solution of CH_2Cl_2/TFA (at 1:1 v/v). The reaction mixture was stirred under nitrogen atmosphere for 2 h. The solution was concentrated in vacuo to afford a colorless oil and purified by flash chromatography using EtOAc/hexane (at 9:1 v/v) to remove the impurities and using CH_2Cl_2/MeOH/NH_3 (at 25:7.3:1 v/v/v) to recover the purified amino lipid product **10** as a colorless oil (0.892g, 1.24 mmol, 83%). R_f [CH_2Cl_2/MeOH/H_2O at 34.5:9:1 v/v/v] 0.43. FTIR: ν_{max} (nujol)/cm^{-1} 3658−3089, 2937, 2871, 1683, 1646, 1541, 1457, 1381, 1253, 1202, 1182, 1133; ^1H NMR (400 MHz, $CDCl_3$/CD_3OD (1/3)) δ_H 0.68 (3H, s, Chol H-18), 0.83, 0.85 (6H, 2d, J = 6.8 and 1.6 Hz), 0.90 (3H, d, J = 6.8 Hz, Chol H-21), 1.00 (3H, s, Chol H-19), 0.93−2.05 (Chol H-1, 2, 4, 7, 8, 9, 11, 12, 14, 15, 16, 17, 20, 22, 23, 25), 2.20−2.34 (2H, m, Chol H-24), 2.44 (2H, t, J = 6.0 Hz, NHCOC$\underline{H}_2$), 3.11 (2H, t, J = 5.2 Hz, C$\underline{H}_2$), 3.19 (2H, t, J = 5.6 Hz, C$\underline{H}_2$), 3.25 (2H, m, C$\underline{H}_2$), 3.57−3.65 (6H, m, 3×C$\underline{H}_2$), 3.65−3.77 (2H, m, C$\underline{H}_2$), 4.38 (1H, m, Chol H-3), 5.37 (1H, m, Chol H-6). ^{13}C NMR (100 MHz, $CDCl_3$) δ_C 11.8 (C-18), 18.7 (C-21), 19.3 (C-19), 21.0 (C-11), 22.5 (C-27), 22.8 (C-26), 23.8 (C-23), 24.3 (C-15), 28.0 (C-25), 28.1 (C-2), 28.2 (C-16), 31.9 (C-8 and C-7), 35.8 (C-20), 36.2 (C-22), 36.6 (C-10), 37.0 (C-1), 38.2 (C$\underline{H}_2$), 38.5 (C-24), 39.5 (C-12 and NHC$\underline{H}_2$CH$_2$NH), 39.7 (C-4), 40.6 (NHC$\underline{H}_2$CH$_2$NH), 42.3 (C-13), 43.1 (C$\underline{H}_2$NH$_2$) 50.1 (C-9), 56.2 (C-17), 56.7 (C-14), 67.2 (C$\underline{H}_2$O), 69.7−70.5 (7×OC$\underline{H}_2$), 74.5 (C-3), 122.4 (C-6), 139.9 (C-5), 157.0 (OCONH), 172.2 (NH(C$\underline{O}$)CH$_2$); m/z ESI-MS [M+H] 721, m/z (FAB + ve) [M+H] 721, FAB-MS calculated for $C_{41}H_{75}N_3O_7$ [M+H] 720.5527, found 720.5543.

N^2-[N'^{31}-*t*Butyloxycarbonyl-(4,7,10,13-tetraoxa-15-aminopentadecanoyl)$_2$]-N^1-cholesteryloxycarbonyl-ethylene-1,2-diamine 11. The amino lipid product **10** (0.591 g, 0.821 mmol, 1 equiv) and the N^{15}-*t*butyloxycarbonyl-4,7,10,13-tetraoxa-15-aminopentadecanoic acid (0.3 g, 0.821 mmol, 1 equiv) were dissolved together in dry CH_2Cl_2 (5 mL) under nitrogen. HBTU (0.467 g, 1.23 mmol, 1.5 equiv) and DMAP (0.3 g, 2.46 mmol, 3 equiv) were added to the solution. The reaction mixture stirred at room temperature under nitrogen for 24 h. The solution was washed successively with citric acid 7% aqueous solution, $NaHCO_3$ aqueous saturated solution and brine before being dried on Na_2SO_4 affording the protected amino-PEG^{350} lipid product **11** as pale orange oil (0.79 g, 0.055 mmol, yield 90%). R_f [CH_2Cl_2/MeOH/H_2O at 34.5:9:1 v/v/v] 0.43. FTIR: ν_{max} (nujol)/cm^{-1} = 3626−3141, 2936, 2868, 1699, 1648, 1541, 1457, 1365, 1253, 1109. ^1H NMR (400 MHz, $CDCl_3$/CD_3OD (1/3)) δ_H 0.69 (3H, s, Chol H-18), 0.86, 0.87 (6H, 2d, J = 6.8 and 2 Hz), 0.92 (3H, d, J = 6.4 Hz, Chol H-21), 1.01 (3H, s, Chol H-19), 1.45 (9H, s, 3×C$\underline{H}_3$), 0.93−2.05 (Chol H-1, 2, 4, 7, 8, 9, 11, 12, 14, 15, 16, 17, 20, 22, 23, 25), 2.20−2.40 (2H, m, Chol H-24), 2.47−2.57 (4H, m, 2×NHCOC$\underline{H}_2$), 3.02 (4H, m, 2×C$\underline{H}_2$), 3.31 (4H, t, J = 5.2 Hz, 2×C$\underline{H}_2$), 3.37 (4H, m, 2×C$\underline{H}_2$), 3.46 (4H, m, 2×C$\underline{H}_2$), 3.55 (2H, t, J = 5.2 Hz, C$\underline{H}_2$), 3.58 (2H, t, J = 5.6 Hz, C$\underline{H}_2$), 3.62−3.67 (12H, m, 6×C$\underline{H}_2$), 3.67−3.78 (4H, m, 2×C$\underline{H}_2$), 4.48 (1H, m, Chol H-3), 5.36 (1H, m, Chol H-6). ^{13}C NMR (100 MHz, $CDCl_3$) δ_C 11.8 (C-18), 18.6 (C-21), 19.2 (C-19),

dx.doi.org/10.1021/bc3004099 | *Bioconjugate Chem.* 2013, 24, 314−332

21.0 (C-11), 22.5 (C-27), 22.7 (C-26), 23.7 (C-23), 24.2 (C-15), 27.9 (C-25), 28.1 (C-2, C-16), 28.3 (3×$\underline{C}H_3$), 31.8 (C-8, C-7), 35.7 (C-20), 36.1 (C-22), 36.5 (2×$\underline{C}H_2$), 36.6 (C-10), 36.7 ($\underline{C}H_2$), 36.9 (C-1), 39.1 ($\underline{C}H_2$), 39.4 (C-24), 39.6−39.7 (C-12, C-4), 40.2 and 40.7 (NH$\underline{C}H_2\underline{C}H_2$NH), 42.2 (C-13), 50.0 (C-9), 56.1 (C-17), 56.6 (C-14), 67.2 (2×$\underline{C}H_2$O), 69.8−70.5 (14×$\underline{C}H_2$), 74.2 (C-3), 78.9 (C quat.), 122.4 (C-6), 139.8 (C-5), 156.2 and 156.6 (O$\underline{C}$ONH), 171.8 and 172.4 (NH($\underline{C}$O)CH_2); *m/z* ESI-MS [M+Na] 1089; *m/z* (FAB +ve) [M^+] 1067, [M+Na] 1089. FAB-MS calculated for $C_{57}H_{103}N_4O_{14}$ [M+H] 1067.7471, found 1067.7479.

N^2-[(4,7,10,13-Tetraoxa-15-amino-pentadecanoyl)$_2$]-N^1-cholesteryloxycarbonyl-ethylene-1,2-diamine 12. The protected amino-PEG^{350} lipid product **11** (0.69g, 0.647 mmol) was dissolved in 10 mL of a solution of CH_2Cl_2/TFA (at 1:1 v/v). The reaction mixture was stirred under nitrogen atmosphere for 2 h. Afterwards the solution was concentrated in vacuo to afford a brown oil. Flash chromatography was used eluting with EtOAc/hexane (at 9:1 v/v) to remove impurities and then the desired product was eluted with MeOH giving purified amino PEG^{350} lipid product **12** as a colorless oil (0.687 g, 0.636 mmol, 95%). R_f [CH_2Cl_2/MeOH/H_2O at 34.5:9:1 v/v/v] 0.43. FTIR: ν_{max} (nujol)/cm^{-1} = 3626−3141, 2936, 2868, 1699, 1648, 1541, 1457, 1365, 1253, 1109; ^{1}H NMR (400 MHz, $CDCl_3$) δ_H 0.68 (3H, s, Chol H-18), 0.86, 0.87 (6H, 2d, *J* = 6.4 and 1.2 Hz), 0.92 (3H, d, *J* = 6.4 Hz, Chol H-21), 1.00 (3H, s, Chol H-19), 0.94−2.07 (Chol H-1, 2, 4, 7, 8, 9, 11, 12, 14, 15, 16, 17, 20, 22, 23, 25), 2.17−2.37 (2H, m, Chol H-24), 2.45−2.56 (2H, m, NHCOC$\underline{H}_2$), 3.10−3.35 (6H, m, 3×C$\underline{H}_2$), 3.53−3.77 (14H, m, 7×C$\underline{H}_2$), 3.78−3.88 (4H, m, 2×C$\underline{H}_2$), 4.35−4.5 (1H, m, Chol H-3), 5.32−5.37 (1H, m, Chol H-6), 7.09 (1H, s br, N−H), 8.03 (3H, s br, N−H and N−H_2). ^{13}C NMR (100 MHz, $CDCl_3$) δ_C 11.7 (C-18), 18.6 (C-21), 19.2 (C-19), 20.9 (C-11), 22.4 (C-27), 22.7 (C-26), 23.7 (C-23), 24.1 (C-15), 27.8 (C-25), 27.9 (C-16), 28.1 (C-2), 31.7 (C-7), 31.8 (C-8), 35.7 (C-20), 35.9 (2×$\underline{C}H_2$), 36.1 (C-22), 36.4 (C-10), 36.9 (C-1), 39.1 ($\underline{C}H_2$), 38.4 (C-24), 39.4 (C-12), 39.6 (C-4), 39.8 and 40.2 (NH$\underline{C}H_2\underline{C}H_2$NH), 42.2 (C-13), 49.9 (C-9), 56.0 (C-17), 56.6 (C-14), 67.0 ($\underline{C}H_2$O), 67.3 ($\underline{C}H_2$O), 69.6−70.1 (15×$\underline{C}H_2$), 74.3 (C-3), 122.2 (C-6), 139.8 (C-5), 156.8 (O$\underline{C}$ONH), 172.4 and 172.7 (NH($\underline{C}$O)CH_2); *m/z* ESI-MS [M+H] 967.

N^2-[N'^{31}-*t*Butyloxycarbonylaminoxyacetyl-(4,7,10,13-tetraoxa-15-aminopentadecanoyl)$_2$]-N^1-cholesteryloxycarbonyl-ethylene-1,2-diamine 13. The amino PEG^{350} lipid **12** (0.637 g, 0.658 mmol, 1 equiv) and *t*-butyloxycarbonyl-aminooxyacetic acid (0.126 g, 0.658 mmol, 1 equiv) were dissolved in dry CH_2Cl_2 (5 mL) under nitrogen. HBTU (0.375 g, 0.988 mmol, 1.5 equiv) and DMAP (0.241 g, 1.976 mmol, 3 equiv) were added to the solution. The reaction mixture stirred at room temperature under nitrogen for 24 h. The solution was washed successively with citric acid 7% aqueous solution and brine before being dried on Na_2SO_4 and the solvent was removed in vacuo. The residue was purified by flash chromatography using successively (CH_2Cl_2/MeOH/H_2O at 78:9:1 v/v/v), (CH_2Cl_2/MeOH/H_2O at 35:9:1 v/v/v), and (CH_2Cl_2/MeOH/AcOH at 92:7:1 v/v/v) rendering Boc-protected aminoxy PEG^{350} lipid **13** as a colorless oil (0.32 g, 0.28 mmol, 43%). R_f [CH_2Cl_2/MeOH/H_2O at 34:5:9 v/v/v] 0.43. FTIR: ν_{max} (nujol)/cm^{-1} = 3626−3141, 2936, 2868, 1699, 1648, 1541, 1457, 1365, 1253, 1109. ^{1}H NMR (400 MHz, $CDCl_3$/CD_3OD 1/3) δ_H 0.69 (3H, s, Chol H-18), 0.86, 0.87 (6H, 2d, *J* = 6.8 and 2 Hz), 0.92 (3H, d, *J* = 6.4 Hz, Chol H-21), 1.01 (3H, s, Chol H-19), 1.45 (9H, s, 3×C$\underline{H}_3$), 0.93−2.05 (Chol H-1, 2, 4, 7, 8, 9, 11, 12, 14, 15, 16, 17, 20, 22, 23, 25), 2.20−2.37 (2H, m, Chol H-24), 2.40−2.48 (4H, m, 2XNHCOC$\underline{H}_2$), 2.95−2.98 (4H, m, 2×C$\underline{H}_2$), 3.16−3.22 (4H, m, 2×C$\underline{H}_2$), 3.34−3.39 (4H, m, 2×C$\underline{H}_2$), 3.42−3.46 (4H, m, 2×C$\underline{H}_2$), 3.51−3.55 (4H, m, 2×C$\underline{H}_2$), 3.57−3.68 (12H, m, 6×C$\underline{H}_2$), 3.67−3.73 (4H, m, 2×C$\underline{H}_2$), 4.25 (2H, s, HNOC$\underline{H}_2$), 4.30−4.45 (1H, m, Chol H-3), 5.29−5.39 (1H, m, Chol H-6). ^{13}C NMR (100 MHz, $CDCl_3$) δ_C 11.8 (C-18), 15.1 ($\underline{C}H_3CH_2O$) 18.7 (C-21), 19.1 (C-19), 21.0 (C-11),) 22.6 (C-27), 22.8 (C-26), 23.8 (C-23), 24.3 (C-15), 28.0 (C-25), 28.1 (C-2), 28.2 (C-16), 30.1 ($\underline{C}H_2$CHN), 31.8 (C-7), 31.9 (C-8), 35.8 (C-20), 36.2 (C-22), 36.6 (C-10), 37.0 (C-1), 38.5 (C-24), 39.6−39.7 ((C-12, C-4), O(CO)NH$\underline{C}H_2\underline{C}H_2$ overlapping), 40.7 (C-4), 42.3 (C-13), 50.0 (C-9), 56.2 (C-17), 56.7 (C-14), 66.7 (O$\underline{C}H_2CH_3$), 67.2 (CH_2O), 72.5 (C-3), 72.8 ((CO)$\underline{C}H_2ONH_2$), 122.6 (C-6), 139.8 (C-5), 151.4 and 151.7 (CH═NO), 158.3 (O$\underline{C}$ONH) and 171.4 (NH($\underline{C}$O)-CH_2ONH_2); ESI-MS [M+Na] 1162.

N^2-[N'^{31}-Aminoxyacetyl-(4,7,10,13-tetraoxa-15-aminopentadecanoyl)$_2$]-N^1-cholesteryloxycarbonyl-ethylene-1, 2-diamine (cholesteryl PEG^{350} aminoxy lipid [CPA]) 6. The Boc-protected aminoxy PEG^{350} lipid **13** (0.05 g, 0.44 mmol) was dissolved in 1.5 mL of isopropanol and 1 mL of a solution of 4 M HCl in dioxane and the reaction mixture was stirred under nitrogen for 2 h. The solvent was concentrated and the residue was precipitated in Et_2O. After successive centrifugation (3500 rpm, 4 °C, 5 min) and change of the Et_2O solution, the solid white residue was dissolved in CH_2Cl_2, concentrated, and dissolved in a mixture of MeCN/H_2O (at 1:1 v/v) and freeze−dried overnight rendering the HCl salt of CPA **6** as an off-white fluffy powder (0.037 g, 0.032 mmol, 73%). HPLC rt 24.69 min or 26.79 min with levulinic acid. R_f [CH_2Cl_2/MeOH/H_2O at 34.5:9:1 v/v/v] 0.43. FTIR ν_{max} (nujol)/cm^{-1} 3661−3122, 2948, 2868, 1701, 1652, 1541, 1470, 1365, 1255, 1108 cm^{-1}; ^{1}H NMR (400 MHz, $CDCl_3$/CD_3OD (1/3)) δ_H 0.68 (3H, s, Chol H-18), 0.84, 0.86 (6H, 2d, *J* = 6.6 and 1.5 Hz), 0.91 (3H, d, *J* = 6.5 Hz, Chol H-21), 1.01 (3H, s, Chol H-19), 0.93−2.04 (Chol H-1, 2, 4, 7, 8, 9, 11, 12, 14, 15, 16, 17, 20, 22, 23, 25), 2.19−2.32 (2H, m, Chol H-24), 2.38−2.53 (4H, m, 2×NHCOC$\underline{H}_2$), 2.95−3.04 (4H, m, 2×C$\underline{H}_2$), 3.17−3.23 (4H, m, 2×C$\underline{H}_2$), 3.23−3.30 (4H, m, 2×C$\underline{H}_2$), 3.35−3.43 (4H, m, 2×C$\underline{H}_2$), 3.43−3.48 (4H, m, 2×C$\underline{H}_2$), 3.50−3.55 (4H, m, 2×C$\underline{H}_2$), 3.55−3.68 (12H, m, 6×C$\underline{H}_2$), 3.68−3.73 (4H, m, 2×C$\underline{H}_2$), 4.33 (2H, s, $HNOCH_2$), 4.59 (1H, s, Chol H-3), 5.30−5.33 (1H, m, Chol H-6). ^{13}C NMR (100 MHz, $CDCl_3$:CD_3OD 1/3) δ_C 12.1 (C-18), 18.9 (C-21), 19.6 (C-19), 21.4 (C-11), 22.7 (C-27), 23.0 (C-26), 24.1 (C-23), 24.6 (C-15), 28.3 (C-25), 28.6 (C-2), and (C-16), 31.8 (C-7) and (C-8), 36.1 (C-20), 36.5 (C-22), 36.8 ($\underline{C}H_2$), 36.9 ($\underline{C}H_2$), 37.0 (C-10), 37.4 (C-1), 38.9 (C-24), 39.4 ($\underline{C}H_2$), 39.6 ($\underline{C}H_2$), 39.9 (C-12), 39.91 ($\underline{C}H_2$), 40.1 (C-4), 40.5 ($\underline{C}H_2$), 42.7 (C-13), 50.5 (C-9), 56.6 (C-17), 57.1 (C-14), 67.6 (2×$\underline{C}H_2$), 69.5 ($\underline{C}H_2$), 70.1 ($\underline{C}H_2$), 70.4−70.84 (12×$\underline{C}H_2$), 72.5 ($\underline{C}H_2ONH_2$), 75.0 (C-3), 122.9 (C-6), 140.2 (C-5), 157.6 (O$\underline{C}$ONH), 173.1, (NH$\underline{C}$O), 174.0 (NH($\underline{C}$O)CH_2ONH_2); *m/z* ESI-MS [M+H] 1040, *m/z* (FAB +ve) [M+Na] 1062.

Preparation of pDNA and siRNA Stock Solutions. Plasmid DNA pUMVC1-nt-beta-gal (pDNA, 7504 bp) was prepared and isolated using the PureLink HiPure Plasmid Filter Purification kit (Invitrogen). The pUMVC1-nt-*β*-gal plasmid was stored thereafter in Tris-HCl/ethylenediamine tetraacetic acid (EDTA) (TE) buffer (500 *μ*L), pH 8.0, and the final

concentration found to be 1.28 μg/μL as measured on a Nanodrop ND-1000 instrument. The plasmid pmarmTTRires-FLuc (gift of Somagenics [Santa Cruz, CA, USA]) was derived from pLucA1[24] with a chimeric gene (iresFLuc) under control of the *att* promoter composed of luciferase (FLuc) downstream of the internal ribosome entry site (ires) of HCV. Upon receipt of the RNAi effector sequences (including siRNAs) from suppliers, sample tubes were briefly centrifuged, then contents were dispersed in nuclease free water to a final concentration of 50 μM then stored at or below −20 °C.

Preparation of Cationic Liposomes, Lipoplex, and ABC Nanoparticles. Lipids were dissolved in chloroform at 5 mg/mL. Appropriate aliquots were combined in a presilanized round-bottom flask (5 mL) to yield cationic liposomes designated **CL1**, **CL2**, and **CL3** (Table 1). In each case, the

Table 1. Lipid Compositions of the Three Cationic Liposome Formulations

molar % of lipid	CL 1	CL2	CL3
CDAN **5**	30	-	-
DODAG **1**	-	20	20
DOPE **2**	50	50	-
DOPC **3**	-	-	50
Chol **4**	-	10	10
CPA **6**	20	20	20

organic solvent was evaporated to dryness to form an even thin lipid film that was further purged with a stream of dry gas to remove residual traces of the organic solvent. The lipid film was hydrated using double distilled H_2O (ddH_2O) to give a multilamellar liposome suspension that was subsequently subjected to sonication in a water bath at 40 °C for 30 min. Post sonication, small unilamellar vesicles (50−80 nm) were diluted to 1.5 mg/mL^{-1} and incubated at room temperature for 15 min. Lipoplex nanoparticles were then prepared by combining liposomes with various volumes of aqueous 4 mM 2-[4-(2-hydroxyethyl)piperazin-1-yl]ethanesulfonic acid (HEPES), pH 7.0−7.4, siRNA solution (50 μM) under heavy vortex to obtain lipoplex nanoparticles (**AB** nanoparticles) of different lipid/siRNA charge ratios (final [siRNA] typically 100 μg/mL; 7 μM).

Thereafter, where appropriate, an aliquot of polyethylene glycol 2000-dialdehyde [PEG^{2000}-$(CHO)_2$, SunBio Ltd., Korea] ([MWt 2000] 2 mg/mL^{-1} in water) was introduced for postcoupling such that final composition of PEG^{2000}-$(CHO)_2$ was between 1 and 5 mol % of total lipid. The pH of solution was monitored by pH boy (Camlab Ltd., Over, Cambridgeshire, UK) and adjusted to pH 4 if required by addition of small aliquots of aqueous solutions of NaOH (0.99 M) or HCl (0.99 M). Post reaction (approx 24 h), the pH was accurately readjusted to pH 7 leaving **ABC** nanoparticles ready for use.

Cationic Liposomes and Lipoplex Nanoparticle Characterization Measurements. Nanoparticles sizes were measured by dynamic scattering (photon correlation spectroscopy ([PCS]) using a Coulter N4+MD submicrometer particle analyzer [Beckman Coulter, UK]). All measurements were performed at 25 °C in ddH_2O, pH 7. Data were recorded at 90° with an equilibrium time of 1 min at individual run times of 2 min. Zeta potential measurements were taken on a Zetasizer Nanoseries Nano-ZS (Malvern Instruments, UK). In each case, total lipid concentrations were set to 1.5 mg/mL^{-1}; [siRNA] varied with lipid/siRNA charge ratio from 0.5 to 10.

Entrapment Efficiency of siRNA. In order to determine the entrapment efficiency of the formulations, siRNA aliquots (50 pmol in 6.65 μL; [siRNA] 100 μg/mL; 7 μM) were placed in Eppendorf tubes and vortex mixed with various added volumes of cationic liposomes solutions (1 mg/mL^{-1}). Lipoplex nanoparticle solutions so formed were then further diluted to 250 μL (final [siRNA] 0.2 μM) and allowed to combine further at room temperature for 30 min. For digestion of surface associated or unentrapped siRNA, 20−30 units of RNase A and 100 units of RNase T were added to lipoplex nanoparticle suspensions. The amount of the enzyme was shown to be sufficient to digest 50 pmol of siRNA (in case more siRNA was needed for the experiments, the amount of enzymes required were adjusted proportionally as required). After incubating for 3 h at 37 °C, the interactions was quenched by adding EDTA to 7 mM. The external bulk medium was separated from the cationic liposomes by gel filtration spin column chromatography. Lipoplex nanoparticles were then solubilized separately with EtOH (250 μL) to release the entrapped siRNA that was subsequently precipitated on ice and incubated with picogreen solution (250 μL) and then incubated at room temperature for 5 min. The fluorescence intensity of each solution was measured at I_{480}/I_{520} nm. The percentage of siRNA entrapped by interactions with cationic liposomes ($\%_{entrap}$) was determined according to changes in initial siRNA fluorescence intensity (I_{siRNA}) post lipoplex nanoparticle entrapment ($I_{siRNA\text{-}NP}$) corrected for nonspecific fluorescence background (I_{NP}) as shown in eq 1:

$$\%_{entrap} = \frac{(I_{siRNA} - [I_{siRNA-NP} - I_{NP}])}{I_{siRNA}} \times 100 \quad (1)$$

Characterization of PEG^{2000}-Dialdehyde Post Coupling. PEG^{2000}-$(CHO)_2$ (27.3 mg, 13.7 μmol) and CPA **6** (14.9 mg, 27.4 μmol) were dissolved in $CDCl_3$ (1.5 mL) in an NMR tube. The reaction mixture was left for 24 h for continuous analysis by ^{1}H NMR spectroscopy. Analytical HPLC was conducted using an aliquot (10 μL) of the reaction mixture diluted in water (190 μL). Postcoupling to lipoplex nanoparticles was investigated in the following way. CDAN **5** (8.51 mg, 14.8 μmol), DOPE **2** (11.0 mg, 14.77 μmol), and CPA **6** (20.5 mg, 19.70 μmol) were combined in $CHCl_3$ and used to prepare CDAN:DOPE:CPA (at 30:50:20, m/m/m) **CL1** cationic liposomes. A thin lipid film was generated by evaporation in vacuo then hydrated with distilled water (6 mL) followed by sonication (5 min). Thereafter, the pH of the resulting liposome suspension was adjusted to 4. A solution of PEG^{2000}-$(CHO)_2$ (19.7 mg, 9.85 μmol) was added and the suspension was again subject to sonication for 10 min. Thereafter, the suspension was stirred gently for 24 h at room temperature then subjected to freeze−drying. Oxime product was isolated by chromatography on silica column using CH_2Cl_2/MeOH (at 19:1 to 9:1 v/v); ^{1}H NMR (400 MHz, $CDCl_3$) 0.68 (6H, s, Chol H-18), 0.83, 0.82 (12H, 2d, J = 6.5 and 2.0 Hz), 0.91 (6H, d, J = 6.4 Hz, Chol H-21), 1.0 (6H, s, Chol H-19), 0.94−2.10 (m, Chol H-1, 2, 4, 7, 8, 9, 11, 12, 14, 15, 16, 17, 20, 22, 23, 25), 2.32 (4H, m, Chol H-24), 2.5 and 2.69 (4H, 2q, J = 5.6 Hz, C$\underline{H_2}$CH═N), 3.31 (8H, m, (CO)NHCH$_2$C$\underline{H_2}$), 3.52 (4H, 2t, J = 5.6 Hz, C$\underline{H_2}$O), 3.64 (260H, m, OCH$_2$C$\underline{H_2}$), 3.81 (2H, m, CH$_2$), 4.4 (4H, m, Chol H-3), 4.5 and 4.6 (4H, 2s, (CO)C$\underline{H_2}$ON═), 4.8 (2H, m, Chol-O(CO)N$\underline{H}$), 5.35 (2H, m, Chol H-6), 6.7 (4H, s br, N−H), 6.8 (2H, s br, N−H), 6.88 and 7.60 (2H, 2t, J = 5.6 Hz, C$\underline{H}$═

dx.doi.org/10.1021/bc3004099 | *Bioconjugate Chem.* 2013, 24, 314−332

N). ^{13}C NMR (100 MHz, $CDCl_3$) 11.8 (C-18). 18.7 (C-21), 19.3 (C-19), 21.0 (C-11), 22.5 (C-27), 22.7 (C-26), 23.8 (C-23), 24.3 (C-15), 26.7 (CH_2), 28.0 (C-25), 28.1 (C-2), 28.2 (C-16), 30.1 ($\underline{C}H_2CHN$), 31.8 (C-7), 31.9 (C-8), 35.8 (C-20), 36.2 (C-22), 36.6 (C-10), 37.0 (C-1), 38.5 (C-24), 39.5−39.7 ((C-12, C-4), O(CO)NH$\underline{C}H_2\underline{C}H_2$ overlapping), 40.7 (C-4), 42.3 (C-13), 50.0 (C-9), 56.1 (C-17), 56.7 (C-14), 61.6 (O$\underline{C}H_2CH_2$), 70.0 and 67.5 (CH_2O), 70.22−70.9 (OCH_2), 72.5 (C-3), 72.8 ((CO)$\underline{C}H_2ONH_2$), 122.4 (C-6),139.8 (C-5), 151.4 and 151.7 (CH═NO), 158.3 (O$\underline{C}$ONH), 171.6 (NH($\underline{C}$O)CH_2ONH_2). R_t = 31 min. This postcoupling and isolation experiment was repeated with **CL2** and **CL3** cationic liposome formulations as well as a demonstration of coupling consistency.

Serum Instability of Nanoparticles. Equal volumes of PEGylated **ABC1**, **ABC2**, and **ABC3** nanoparticles prepared with a fixed lipid/siRNA charge ratio of 4 in water (1 mg/mL) and bovine or fetal calf serum (FCS) were mixed to a total volume (1 mL) and incubated in a water bath at 37 °C. Final serum concentration was 80% v/v, final lipid concentrations 0.5 mg/mL; [siRNA] 3 μM. Samples of each nanoparticle made up in FCS 80% v/v, at the same concentrations as above, were incubated at 37 °C in a water bath and values of A_{600} absorbance were determined at 30 min intervals over 4 h on a UV−vis spectrometer. Each value of A_{600} absorbance determined was corrected for background A_{600} absorbance measured from a corresponding time matched control incubation comprising only FCS 80% v/v in ddH_2O.

Triggered Release Studies. The stabilities of 5 mol % PEGylated **ABC1**, **ABC2**, and **ABC3** nanoparticle formulations were studied at different conditions of pH and siRNA release analyzed for by gel electrophoresis (Novex 20% Tris-Borate/EDTA [TBE] gels, Invitrogen). Nanoparticles were prepared from aliquots of siRNA (150 pmol; 2 μg in 10 μL water) in Eppendorf tubes (0.5 mL) to which were added aliquots from stock solutions (2 mg/mL) in water of control cationic liposomes or aminoxy cationic liposomes **CL1**, **CL2**, or **CL3** as appropriate for the formation of lipoplex nanoparticles with a lipid/siRNA charge ratio of 4. All samples were vortex mixed for 30 s, incubated at room temperature for 30 min then PEG^{2000}-$(CHO)_2$ aliquots were added to ensure the formation of 5 mol % **ABC1**, **ABC2**, and **ABC3** nanoparticles. Individual samples were pH corrected and controlled to 4, 5.5, or 7.4, then incubated at 37 °C for 120 min. Aliquots (5 μL) were taken from each nanoparticle mixture at 30, 60, and 120 min and mixed with of Novex TBE Hi-Density Sample Buffer (5×) (2 μL). Each mixture was applied by pipet into the individual wells of gels run at 200 V for 30 min. SYBR Green was used to stain the gels for the presence of naked or released siRNA. **ABC$_{control}$** control nanoparticles were prepared with the requisite formulation, CDAN/DOPE/CPA/MeO-PEG^{2000}-DSPE (at 30:45:20:5 m/m/m/m), according to the procedure above minus the chemical postcoupling step.

In Vitro Gene Knockdown Studies. Three different cell lines: HeLa, HepG2, and Huh7 were seeded then incubated at 37 °C with 5% CO_2 till 70−80% confluent (approx 10^4−10^5 cells/well). For the exogenous gene knockdown experiments involving HeLa and Huh7 cells, these cell lines were subject to nonviral transfection with β-galactosidase (β-gal) expressing plasmid pUMVC1-nt-β-gal introduced by Trojene (Avanti Polar Lipid Inc.) cationic liposomes, according to manufacturer's instructions. The lipid/pDNA ratio in each case was 12:1 w/w and transfection times of 3 h only were used. Post transfection, cells were washed with PBS twice in preparation for siRNA gene knockdown experiments. For exogenous gene knockdown experiments using HepG2 cells, these cell lines were subject to viral transfection using replication defective adenovirus vector (AdRSVLacz). Transduction was carried out in 48-well plate format with 4×10^6 cells/well maintained in small volumes (each 150 μL) of complete growth medium (Dulbecco's Modified Eagle's Medium [DMEM], 10% FCS and, 1% penicillin, and streptomycin). The viral particles were added to each well at multiplicity of infection (MOI) of 10. Post transduction, cells were incubated for 18 h, then the transduction medium was replaced with fresh growth medium. Thereafter, cells were washed with PBS twice once again in readiness for siRNA-mediated gene knockdown.

PEGylated **ABC1**, **ABC2**, or **ABC3** nanoparticle suspensions were then prepared with lipid/siRNA charge ratios of 4 using either a functional anti-β-gal siRNA or a control siRNA sequence. Aliquots of different size were then administered to cultured cells, prepared as above for exogenous β-gal expression, in order for cells to experience a range of different single siRNA doses/well (varied from 1 to 10 pmol/well, as indicated). In each case, cells were subject to a period of 3 h in Optimem at 37 °C, 5% CO_2, for siRNA delivery (siFection). Thereafter, nanoparticle suspensions were removed and replaced by cell growth medium. Cells were then incubated for a further 30 h prior to analysis of β-gal enzyme activity levels in cells post siRNA delivery. Post cell lysis, β-gal enzyme activity levels per well were then measured with a standard β-gal enzyme colorimetric assay system and normalized according to the protein content per lyzate per well as per standard bicinchoninic acid (BCA) assays.

For the endogenous gene knockdown experiments involving HepG2 and Huh7 cells, cells were seeded 500 cells/well in 96-well plates. Cells were then allowed to grow until 70% confluent. PEGylated **ABC1**, **ABC2**, or **ABC3** nanoparticle suspensions (with or without **ABC$_{control}$** nanoparticles as indicated) were prepared all with lipid/siRNA charge ratios of 4 using either a functional antiglyceraldehyde-3-phosphate dehydrogenase (GAPDH) siRNA or a control siRNA sequence (KDalert assay, Ambion, USA). Aliquots of different size were then administered to cultured cells, in order for cells to experience a range of different single siRNA doses/well (varied from 2 to 8 pmol/well, as indicated). In each case, cells were subject to a period of 4 h in Optimem at 37 °C, 5% CO_2, for siRNA delivery. Thereafter, nanoparticle suspensions were removed and replaced by DMEM/FCS cell growth medium. Cells were then incubated for a further 48 h prior to analysis of GAPDH levels in cells post siRNA delivery (KDalert assay for GAPDH protein concentration).

In Vitro Cellular Uptake Assays. The cellular uptake of **ABC** nanoparticles was investigated using fluorescence-activated cell sorting (FACS) analysis. Prior to FACS analysis, cells (HepG2 in this case) were seeded in 6-well plates and grown in DMEM media, supplemented with 10% FCS and 1% penicillin−streptomycin. Cells were then incubated at 37 °C, 5% CO_2, until 80% confluent. Subsequently, cells were treated with a range of PEGylated **ABC1**, **ABC2**, **ABC3**, and **ABC$_{control}$** nanoparticles each comprising a lipid/siRNA charge ratio of 4 (and each containing fluorescein [FAM]-labeled siRNA). In each case, [siRNA] was 20 pmol/well. After 4 h, the cells were washed with PBS (2 mL/well) then incubated with trypsin solution (1 mL) at 37 °C until cells were detached from their respective wells. Thereafter, DMEM (3 mL) was added to each

well and cells suspended. Cells were reduced to pellet by centrifugation (50 000*g*, 5 min), then each pellet was separately resuspended in ice−cold PBS (300 μL) and transferred to individual FACS tubes (Elkay Laboratory Products, UK Ltd., Basingstoke, UK). The FACS tubes were loaded into a FACS Calibur machine (Becton Dickinson), which was set up to analyze 10 000 cells/sample. Finally results were analyzed using *WinMDI* software (v 2.8). Cellular fluorescence was analyzed by cytometer and presented graphically as a plot of side scatter (SSC) against fluorescence (FL1). Relative cellular uptake was presented as a percentage of the theoretical maximum.

Effect of Cellular Pathway Inhibitors on Functional siRNA Delivery. HepG2 cells were seeded in 6-well plates and grown in DMEM media, supplemented with 10% FCS and 1% penicillin−streptomycin. Cells were then incubated at 37 °C, 5% CO_2, until 80% confluent. Subsequently, cells were pretreated with either nocodazole (10 μM), genistein (200 μM), chlorpromazine (56 μM), 5-(*N*,*N*-dimethyl) amiloride hydrochloride (10 μM), or carbobenzoxy-D-phenylalanine-L-phenylalanine-glycine (ZfFG) (50 μM) (all from Sigma) in serum-free culture medium for 1 h, at 37 °C, 10% CO_2. Cells were then washed and treated for 2 h prior to FACS analysis (see above) with **AB1**, **AB2**, or **AB3** lipoplex nanoparticles or 5 mol % **ABC1**, **ABC2**, or **ABC3** nanoparticle suspensions ([siRNA] was 20 pmol/well). All nanoparticles were prepared with lipid/siRNA charge ratios of 4 and each was labeled with 0.5 mol % dioleoyl-L-α-phosphatidylethanolamine-*N*-(lissamine rhodamine B sulphonyl) (DOPE-Rhoda) fluorescent lipid. Thereafter, the extent of nanoparticle assisted siRNA-mediated gene knockdown was determined by treating cells with **AB1**, **AB2**, or **AB3** lipoplex nanoparticles or 5 mol % **ABC1**, **ABC2**, or **ABC3** nanoparticle suspensions ([siRNA] was 8 pmol/well). In this case all nanoparticles were prepared with lipid/siRNA charge ratios of 4 using either a functional anti-GAPDH siRNA or a control siRNA sequence (KDalert assay, Ambion, USA). Cells were assessed for GAPDH protein levels (KDalert assay for GAPDH protein concentration).

Fluorescence and Confocal Microscopy. HepG2 cells were grown in DMEM supplemented with 10% FCS and 1% penicillin−streptomycin, in a 6-well plate (10^5 cells per well in 2 mL of complete media) fitted with glass coverslips at 37 °C, 10% CO_2. Cells were grown until 80% confluent and the media was then removed and replaced with fresh complete media (2 mL/well). Cells were then treated with 5 mol % **ABC1**, **ABC2**, or **ABC3** nanoparticles (lipid concentration 20 μg/well; siRNA 100 pmol/well), labeled with 0.5 mol % DOPE-Rhoda fluorescent lipid), for 3 h at 37 °C, 10% CO_2. Thereafter, cells were washed with phosphate-buffered saline (PBS) (×2) then treated with 0.4% (w/v) trypan blue solution in Hanks balanced salt solution (HBSS) to quench the extracellular fluorescence. Cells were washed once again with PBS (×2) then fixed with paraformaldehyde (PFA) (15 min at 37 °C). Microscopy images were obtained on an Olympus 251 microscope, and confocal images were obtained using a Leica upright confocal microscope. For colocalization studies, 80% confluent cells were treated with 5 mol % **ABC1**, **ABC2**, or **ABC3** nanoparticles (20 μg/well) together with Alexa 488-labeled transferrin (5 μg/mL) or Alexa 488-labeled cholera toxin B (1 μg/mL) in serum free media (2 mL/well) for 60 min. Cells were then processed for microscopy as above.

In Vivo Biodistribution of PEGylated siRNA Nanoparticles. A cohort of 3 female MF1 mice were injected i.v. with either saline or 5 mol % **ABC2** nanoparticles incorporating DOPE-Rhoda labeled lipid and Alexa 488-labeled siRNA (administered dose 3 mg/kg animal body weight). At 24 h post nanoparticle administration, animals were sacrificed, and liver, kidney, spleen, and lung tissues were harvested and fixed for 16 h at 4 °C in 4% PFA in PBS. Tissues were then placed in 10% sucrose in PBS for 16 h at 4 °C, washed with PBS, and then snap-frozen in liquid nitrogen and stored at −80 °C. Slices (10 mg) from each tissue were homogenized in tissue lysis buffer (500 μL). Aliquots (10 μL) of individual tissue lysate were further diluted into PBS (500 μL), then sample subaliquots (100 μL) were removed to evaluate both the extent of Rhodamine fluorescence intensity and protein content by means of a BCA assay and plate reader. Alternatively, snap-frozen stored liver tissue was cut to 7 μm sections by means of a Cryostat, then collected onto APES coated glass slides. Sections were dried for 1 h at room temperature before storage at −20 °C for up to two weeks. Sections were examined and photographed using standard fluorescence and confocal microscopy, using the same settings for each treatment group. A routine histological study was also carried out on formalin-fixed optimal cutting temperature (OCT)-embedded liver tissue samples. These liver tissue samples were cut into 4 μm sections, and dehydrated through a series of decreasing concentrations of ethanol. The sections were then stained with hematoxylin and eosin to observe liver morphology.

In Vivo Delivery of RNAi Effectors. In the first main experiment, male MF1 mice (1−2 months old, 25−30 g body weight) (B&K Universal Ltd., UK) were treated with plasmid pLucA1 by the murine hydrodynamic injection (MHI) protocol[24] (single 5−8 s tail vein injection with plasmid pLucA1 (5 μg) dispersed in PBS [2.5 mL]). The resulting MHI-mice express the luciferase gene in their liver at exceptional levels for months without any sign of plasmid integration or silencing, except through hepatocyte turnover. One week post MHI protocol consistent with previous protocols,[25] 5 mol % **ABC2** nanoparticles were prepared with antiluciferase siRNA (purchase from Qiagen) or control siRNA (Silencer negative control siRNA purchased from Applied Biosystems/Ambion) and administered to the MHI mice (typically $n = 6$) by tail vein injection (200 μL, siRNA dose 1 mg/kg animal body weight) in 10% sucrose solution. Other controls were 10% sucrose solution alone and 5 mol % $\mathbf{ABC}_{\mathbf{control}}$ nanoparticles prepared using DODAG/Chol/DOPE/CPA (at 20:10:45:20 m/m/m/m) cationic liposomes and 5 mol % "(ω-methoxy-polyethylene glycol 2000)-*N*-carboxydistearoyl-L-α-phosphatidylethanolamine (MeO-PEG^{2000}-DSPE) with the same antiluciferase siRNA (purchase from Qiagen).

In the second main experiment, male MF1 mice (1−2 months old, 25−30 g body weight) (B&K Universal Ltd., UK) were treated with plasmid pmarmTTRiresFLuc by the murine hydrodynamic injection (MHI) protocol[24] (single 5−8 s tail vein injection with plasmid pmarmTTRiresFLuc (5 μg) dispersed in PBS [2.5 mL]). At, 1 week post MHI, 5 mol % **ABC2** nanoparticles were prepared with anti-iresHCV short stem, small hairpin RNA (sshRNA) or control sshRNA (supplied by Somagenics, Santa Cruz, CA, USA),[26,27] and administered to the MHI mice (typically $n = 6$) by tail vein injection (200 μL, sshRNA dose 1 mg/kg or less as indicated) in 10% sucrose solution. Other controls were naked anti-iresHCV sshRNA administered at the same dose and 5 mol % **BC2** cationic liposomes ("empty liposomes") administered at

dx.doi.org/10.1021/bc3004099 | *Bioconjugate Chem.* 2013, 24, 314−332

the corresponding equivalent dose of lipid administered with 5 mol % **ABC2** nanoparticles above.

For either main experiment, post tail vein injections murine liver-localized luciferase expression was monitored regularly at 24 h intervals as follows. Mice were injected intraperitoneal (i.p.) with D luciferin solution (300 μL, 15 mg/mL in PBS), anaesthetised by Isoflurane, and then liver-generated luciferase bioluminescence was observed by means of an IVIS Imaging 50 device (Xenogen). Imaging was performed in a light-tight chamber on a temperature-controlled, adjustable stage, while Isoflurane was administered by means of a gas manifold at a flow rate of 2% v/v. Images were acquired at a medium binning level, with a 20 cm field of view and an acquisition time of 60 s. Bioluminescence from liver-localized luciferase catalyzed conversion of luciferin was reported as photons/s/cm^2/sr. The auto function was used to define the minimum and the maximum for the scale at each time point. Data were analyzed using the *LivingImage 2.5* software (Xenogen).

Data Analysis. All data are presented as the mean plus/minus standard error. Means were compared using significance calculated using unpaired Student's *t*-tests. The probability values $P < 0.05$ were marked with * $P < 0.01$ were marked with **.

RESULTS

Initially, three cationic liposome formulations were prepared (Table 1). The constituent lipids used in their relative mol ratios are shown (Figure 1). Central to the preparation of all three formulations was the use of a CPA lipid **6** used in our previous work concerning the development and use of a putative pH-triggered PEGylated siRNA-nanoparticle system (siFECTplus).[14] Here, we report a revised and updated synthesis of CPA **6** (Scheme 2). All three cationic liposome formulations comprise a lipid composition related to siFECTplus. Of these, Cationic liposome 1 (**CL1**) was prepared with the same cationic lipid CDAN **5** and so is most closely related to siFECTplus. Cationic liposome 2 (**CL2**) and Cationic liposome 3 (**CL3**) were prepared with the alternative cationic lipid DODAG **1** (Figure 1).[13] Our objective was to employ all three cationic liposome formulations separately to formulate a set of contrasting pH-triggered PEGylated siRNA-nanoparticle prototypes based on the aminoxy-PEG aldehyde coupling reaction methodology, described previously.[14] Systematic studies were then to be performed, described as follows, in order to attain an improved appreciation of structure and mechanisms that might suggest potential ways to improve the efficacy of nanoparticle mediated RNAi-functional delivery in future work.

siRNA Lipoplex Formation. Fixed siRNA concentrations (50 μM) were combined with varying concentrations of **CL1**, **CL2**, or **CL3**, under rapid vortex mixing conditions in 4 mM HEPES buffer, pH 7.0−7.4 (final [siRNA] typically 100 μg/mL; 7 μM). The diameters of resulting siRNA-lipoplex nanoparticles were then determined by PCS plotted out as a function of lipid/siRNA charge ratio. In doing this, charge ratio was determined assuming a net charge of +1.7 per CDAN or DODAG molecule, based upon previous experience and measurements.[13,21,28] Results are shown (Figure 2A,B) and are in accord with variations in diameters of pDNA-lipoplex nanoparticles formed from the combination of pDNA with cationic liposomes under comparable conditions.[13] In particular, the variation in nanoparticle diameter as a function of lipid-siRNA charge ratio appears to form into three zones (right to left), the first presumed to comprise siRNA-lipoplex nanoparticles with a negative overall charge, the second to comprise of nanoparticles with a neutral overall charge, and the

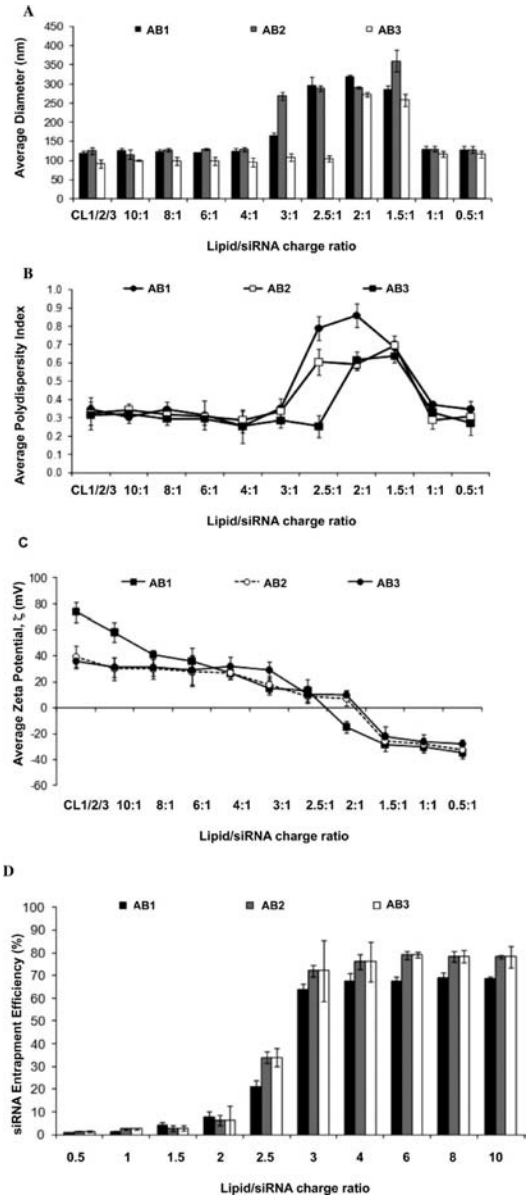

Figure 2. Physical characterization of lipoplex nanoparticles as a function of their lipid/siRNA charge ratios. **AB1**, **AB2**, and **AB3** lipoplex nanoparticles were obtained by mixing the cationic liposomes **CL1**, **CL2**, and **CL3**, respectively, with siRNA at different lipid/siRNA charge ratios ([lipid] 1.5 mg/mL throughout unless otherwise stated): (A) Diameters of lipoplex nanoparticles, formulated with decreasing charge ratios were measured using photon correlation spectroscopy. Size measurements were made 1 h postmixing. (B) Size distribution of the lipoplex nanoparticles formulated with decreasing lipid/siRNA charge ratios. (C) Average ζ potential of **AB1**, **AB2**, and **AB3** lipoplex nanoparticles formulated from cationic liposomes **CL1**, **CL2**, and **CL3**, respectively, with decreasing lipid/siRNA charge ratios. (D) Entrapment efficiencies of siRNA by cationic liposomes **CL1**, **CL2**, and **CL3**, respectively, as determined using fluorescence exclusion assays. Aliquots of siRNA (50 pmol) were combined with indicated cationic liposomes at different lipid/siRNA charge ratios (final [siRNA] 0.2 μM). Free siRNA was digested then entraped siRNA estimated by the addition of a nucleic acid-responsive fluorescent dye. Extent of siRNA entrapment was expressed as a percentage of the theoretical maximum.

dx.doi.org/10.1021/bc3004099 | *Bioconjugate Chem.* 2013, 24, 314−332

Scheme 3. Schematic Illustration of the Post-Coupling Method for Assembling pH-Triggered PEGylated siRNA-Nanoparticles (pH-triggered siRNA-ABC nanoparticles)

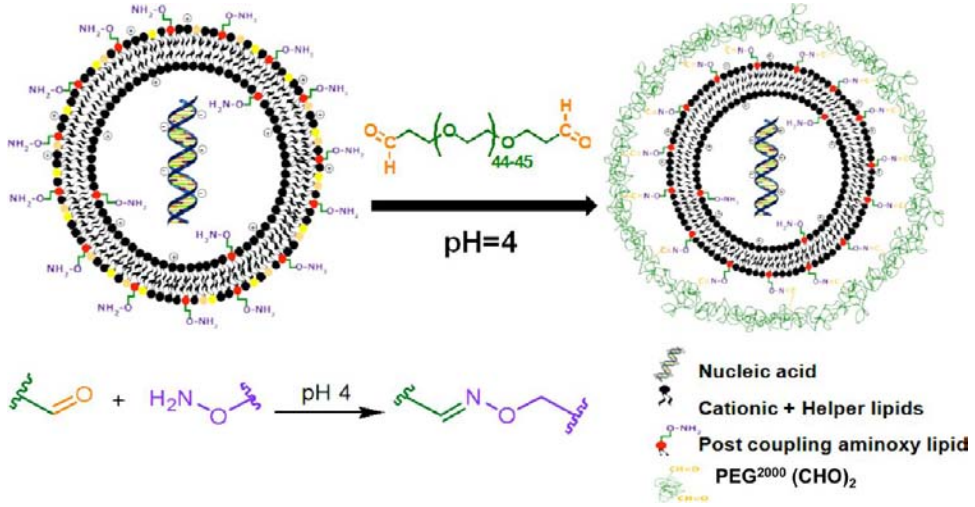

third of nanoparticles with a positive overall charge. The putative charge status of lipoplex nanoparticles in each zone was confirmed by means of average zeta potential measurements (Figure 2C). Thereafter, siRNA entrapment efficiency was investigated by means of the pico-green fluorescence assay (final [siRNA] 0.2 μM) (Figure 2D). When cationic liposomes and siRNA interact, a complex mixing process takes place, leading to siRNA entrapment inside a dense lipid-nucleic acid nanoparticle, thereby rendering siRNA inaccessible to pico-green intercalation and hence preventing the generation of a fluorescence signal. Where siRNA is not entrapped, intercalation becomes possible leading to a fluorescence signal. Our data indicated that siRNA lipoplex nanoparticle formulations prepared with lipid-siRNA charge ratios of about 3 (ζ potentials +20−40 mV) were capable of siRNA entrapment of >80% efficiency.

siRNA Lipoplex Nanoparticle Cellular Uptake, Stabilities, and Toxicities. The cellular uptake efficiencies of siRNA lipoplex nanoparticles prepared from **CL1**, **CL2**, and **CL3** (named **AB1**, **AB2**, and **AB3** nanoparticles, respectively) were then compared by means of fluorescence labeling (using FAM-labeled siRNA) and fluorescence activated cell sorting (FACS) (Supporting Information Figure S1). In all cases, 90% cellular uptake required nanoparticles with a lipid/siRNA charge ratio of at least 4 if not higher. Cellular toxicity effects were evaluated using the lactate dehydrogenase (LDH) release assay. Within experimental error, even up to 12 h of exposure, minimal cytotoxicity was observed from cellular exposure to **AB1**, **AB2**, and **AB3** nanoparticles (final [siRNA] 20 pmol/well) even with when lipid/siRNA charge ratios were as high as 8 (Supporting Information Figure S2A). However, if cells were allowed to grow for 24 h post exposure to **AB1**, **AB2**, and **AB3** nanoparticles, then cytotoxic effects were observed when lipid/siRNA charge ratios were as low as 6 as well as 8 (Supporting Information Figure S2B). Given the sum total of this data and data of the previous section, then **AB1**, **AB2**, and **AB3** nanoparticles with a lipid/siRNA charge ratio of 4 (that corresponds with a 12:1 w/w lipid/siRNA ratio) appeared to possess the most optimal combination of characteristics including minimal cellular toxicity. Therefore, only these siRNA-lipoplex nanoparticles were used in subsequent experiments.

PEGylation of siRNA Lipoplex Nanoparticle Formulations. In line with our previous publication,[14] PEGylation of **AB1**, **AB2**, and **AB3** lipoplex nanoparticles, presenting aminoxy functional groups (due to inclusion of CPA lipid **6**), was achieved by incubation with appropriate mol % amounts of PEG^{2000}-dialdehyde (giving **ABC1**, **ABC2**, and **ABC3** nanoparticles, respectively). PEG postcoupling was mediated by oxime bond formation at pH 4.0 (Scheme 3). Coupling reactions could be monitored by HPLC during reaction (oxime product appears at t_R = 30 min; see Experimental Section for conditions), and we were also able to isolate successfully and characterize a PEG lipid oxime conjugate by ^{1}H NMR spectroscopy after a 24 h incubation period at ambient temperature (see Experimental Section). As noted previously,[14] coupling was found to take place typically over a period of 16−24 h. The effect of PEGylation on **ABC1**, **ABC2**, and **ABC3** nanoparticle diameters and on measured ζ-potential values as compared to parent **AB1**, **AB2**, and **AB3** lipoplex nanoparticles (lipid/siRNA charge ratio of 4 in all cases) was determined as a function of different levels of surface PEG from 1 to 5 mol % (Figure 3A,B). Higher PEGylation levels virtually eliminated ζ-potential values from +30 to 40 mV, in the case of **AB2** and **AB3** lipoplex nanoparticles, to approx +5 mV in the case of corresponding 4 and 5 mol % **ABC2** and **ABC3** nanoparticles. These higher levels of PEGylation also resulted in profound effects on nanoparticle stabilities with respect to colloidal aggregation in 50% and 80% serum stability assays (Figure 4 and Supporting Information Figure S3). **AB1**, **AB2**, and **AB3** lipoplex nanoparticles and corresponding 1−3 mol % **ABC1**, **ABC2**, and **ABC3** nanoparticles were unstable with respect to aggregation over time in both environments. By contrast, 4 and 5 mol % **ABC1**, **ABC2**, and **ABC3** nanoparticles were completely stable over 250 min in 50% serum conditions (Supporting Information Figure S3), although only 5 mol % **ABC1**, **ABC2**, and **ABC3** were colloidally stable over the same time period in 80% serum conditions (Figure 4).

Triggerability with pH Change Observed with 5 mol % PEGylated siRNA-Nanoparticles. In order to investigate the pH-triggered characteristics of 5 mol % PEGylated siRNA-nanoparticles, a series of assays were performed in which samples of 5 mol % **ABC1**, **ABC2**, and **ABC3** nanoparticles ([siRNA] 15 μM in each case) were incubated at pH 7.4, 5.5,

dx.doi.org/10.1021/bc3004099 | *Bioconjugate Chem.* 2013, 24, 314−332

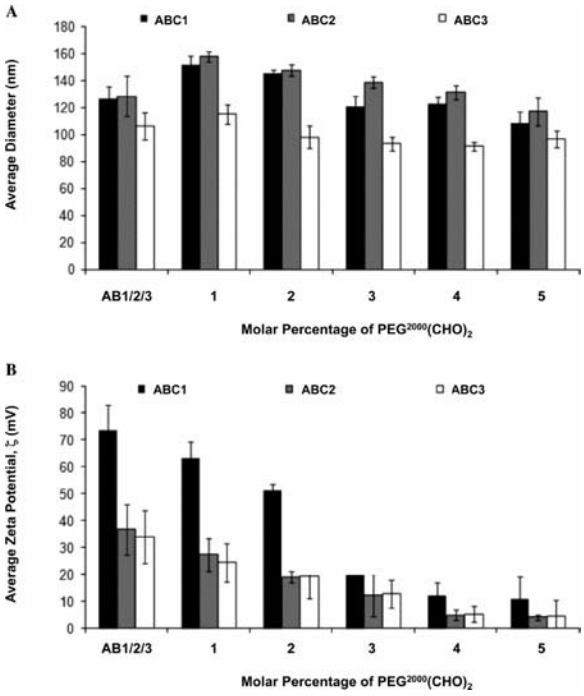

Figure 3. (A) Average diameter of **AB1**, **AB2**, and **AB3** lipoplex nanoparticles and their corresponding PEGylated nanoparticle variants **ABC1**, **ABC2**, and **ABC3** as determined by photon correlation spectroscopy (PCS). The lipoplex nanoparticles were prepared at the lipid/siRNA charge ratio of 4 and incubated with increasing mol % values of PEG^{2000}-$(CHO)_2$ at pH 4 for a minimum of 16−24 h in order for the post coupling reaction to take place. HPLC was used to monitor the reaction. The pH of the resulting PEGylated siRNA-nanoparticles was adjusted to 7.4 then PCS was used to determine their size. (B) Average ζ potential of **AB1**, **AB2**, and **AB3** lipoplex nanoparticles and their corresponding PEGylated nanoparticle variants **ABC1**, **ABC2**, and **ABC3** nanoparticles prepared as in (A) and then characterized by a zeta sizer instrument (Malvern Zetasizer) ([lipid] 1.5 mg/mL throughout).

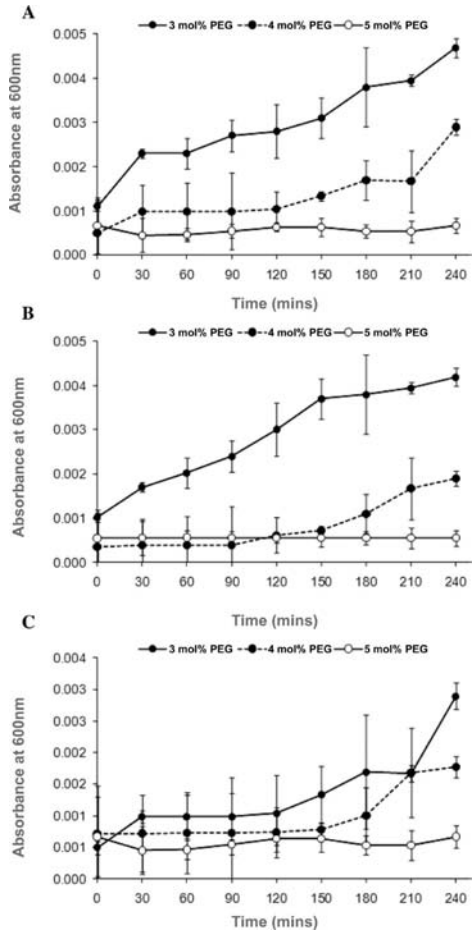

Figure 4. Stability of **ABC1**, **ABC2**, and **ABC3** nanoparticles formulated with lipid/siRNA charge ratios of 4 and incubated in 80% FCS, as assessed by differential absorbance at A_{600}. Nanoparticle stability was assessed by monitoring the increase in light scattering of nanoparticle suspensions as a function of time (final [siRNA] 3 μM). (A) Stability of **ABC1** nanoparticles. (B) Stability of **ABC2** nanoparticles. (C) Stability of **ABC3** nanoparticles.

and 4.0 for 30, 60, and 120 min at 37 °C; after which siRNA release was detected by gel electrophoresis (Figure 5). Control PEGylated siRNA-nanoparticles (5 mol % $\mathbf{ABC_{control}}$) were prepared for comparison that were formulated by a post-modification strategy. This was achieved by combining siRNA with cationic liposomes composed of CDAN/DOPE/CPA at 30:45:20 (m/m/m) to form $\mathbf{AB_{control}}$ lipoplex nanoparticles that were then incubated with the PEG-lipid MeO-PEG^{2000}-DSPE (5 mol %) to give the desired 5 mol % $\mathbf{ABC_{control}}$ nanoparticles. These 5 mol % $\mathbf{ABC_{control}}$ nanoparticles represent an important PEGylated siRNA-nanoparticle control devoid of the oxime linkages formed by postcoupling. The 5 mol % **ABC1**, **ABC2**, and **ABC3** nanoparticles were all found uniformly stable at pH 7.4 and pH 4.0 but enabled the release of siRNA at pH 5.5 in 30 min. By comparison, 5 mol % $\mathbf{ABC_{control}}$ nanoparticles were essentially unable to release siRNA at pH 5.5 over 120 min. In addition, we observed that 5 mol % **ABC1**, **ABC2**, and **ABC3** nanoparticles were also enabled to release siRNA more modestly at pH 6.0 (data not shown).

Functional Delivery of siRNA to Cells in Vitro. Initial uptake experiments were performed with HeLa cells. 1 mol % **ABC1**, **ABC2**, and **ABC3** nanoparticles (lipid/siRNA charge ratio 4) were prepared from **CL1**, **CL2**, and **CL3** cationic liposome formulations respectively labeled with 0.5 mol % DOPE-Rhoda. 1 mol % **ABC1** nanoparticles with the highest overall ζ-potential (Figure 3B) were taken up most rapidly in the first 60 min. However, after 120 min, all three nanoparticles were found taken up to equivalent extents (see Supporting Information Figure S4). Functional delivery of siRNA in vitro was then investigated with both exogenous and endogenous gene targeting assays.

The exogenous gene target selected was β-gal. HeLa cells and liver cell lines Huh7 were subject to transfection with the β-gal expressing plasmid pUMVC1-nt-β-gal, in a process mediated by Trojene (Avanti Polar Lipid Inc.). HepG2 cells were prepared for β-gal expression by adenovirus mediated gene transduction. After preparation, cells were washed and tested for β-gal activity levels prior to the administration for 3 h of 1 mol % **ABC1**, **ABC2**, and **ABC3** nanoparticles that were previously prepared with lipid/siRNA charge ratios of 4 and with either anti-β-gal siRNA or the corresponding control siRNA sequence. Cells were then washed once more and knockdown of β-gal levels was then determined after a further 30 h of cell incubation. Data are consistent in showing that >90% specific knockdown could be achieved in β-gal levels at siRNA doses of 6 pmol/well ([siRNA] concentration 6 nM) or higher, in all of the three different cell lines evaluated (Figure 6A,B,C).

dx.doi.org/10.1021/bc3004099 | *Bioconjugate Chem.* 2013, 24, 314−332

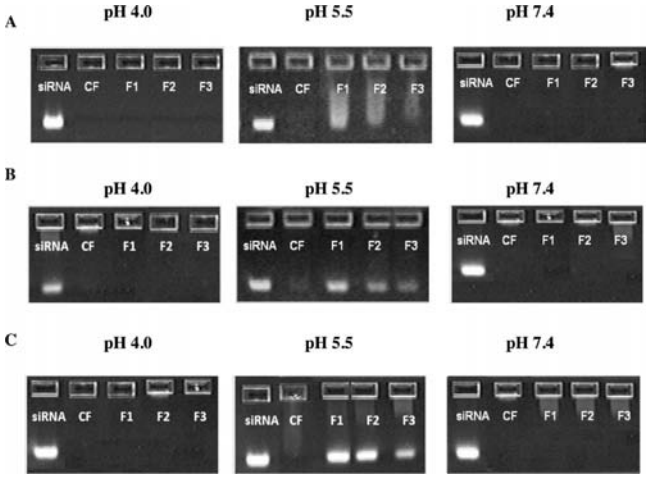

Figure 5. Gel electrophoresis of 5 mol % PEGylated siRNA nanoparticles following incubation (siRNA, 150 pmol/incubation) in buffered solutions at pH values 4.0, 5.5, and 7.4. **CF** = 5 mol % **ABC**$_{control}$, F1 = 5 mol % **ABC1**, F2 = 5 mol % **ABC2**, F3 = 5 mol % **ABC3**. (A) Gels following 30 min incubation in buffer solutions, (B) gels after 60 min incubation, and (C) gels after 120 min of incubation at the different pH values. Aliquots of siRNA added per lane were approx 3 pmol/well.

The selected endogenous gene target was GAPDH making use of the KDalert knockdown assay kit (Ambion). GAPDH knockdown studies were performed with Huh7 and HepG2 cells. Cells were administered for 4 h with 1 mol % **ABC1**, **ABC2**, and **ABC3** nanoparticles that were previously prepared with lipid/siRNA charge ratios of 4 and with either anti-GAPDH siRNA or the corresponding control siRNA sequence. Cells were then washed and relative GAPDH knock down levels were then determined after a further 48 h of cell incubation. The 1 mol % **ABC2** nanoparticles were found to mediate the highest levels of specific GAPDH knockdown in both cell lines at all siRNA doses of 2, 4, or 8 pmol/well. The 1 mol % **ABC2** nanoparticles were also able to mediate levels of specific knockdown at least 80% and 90%, in HepG2 and Huh7 cells, respectively, at the highest dose of siRNA used of 8 pmol/well (Figure 6D,E). Furthermore, 1 mol % **ABC2** nanoparticles were also found to mediate at least 60% specific knockdown of GAPDH levels in primary murine hepatocytes once again at the highest dose of siRNA used of 8 pmol/well (data not shown).

The same endogenous gene target assay was then used to assess the impact of increased PEGylation on **ABC1**, **ABC2**, and **ABC3** nanoparticles. We prepared samples of 1, 2, 3, 4, and 5 mol % versions of **ABC1**, **ABC2**, and **ABC3** nanoparticles, alongside appropriate **ABC**$_{control}$ nanoparticles (as above), with lipid/siRNA charge ratios of 4 and with either anti-GAPDH siRNA or the corresponding control siRNA sequence. Cellular uptake was assessed in parallel by FACS analysis (see Supporting Information Figure S1 for reference). The cellular uptake of higher mol % PEGylated siRNA-nanoparticles was observed to be reduced only modestly in HepG2 cells relative to the lower mol % PEGylated siRNA-nanoparticles (from >80% to approx 60%) (Figure 7A). However, increased PEGylation did impair substantially the capacity of **ABC**$_{control}$, and to some extent **ABC3** nanoparticles, to mediate specific GAPDH knockdown in a proportionate manner in the same HepG2 cells. In contrast, higher levels of PEGylation did not appear to impair substantially the efficiency of **ABC1** or **ABC2** nanoparticle-mediated specific knockdown of GAPDH in the

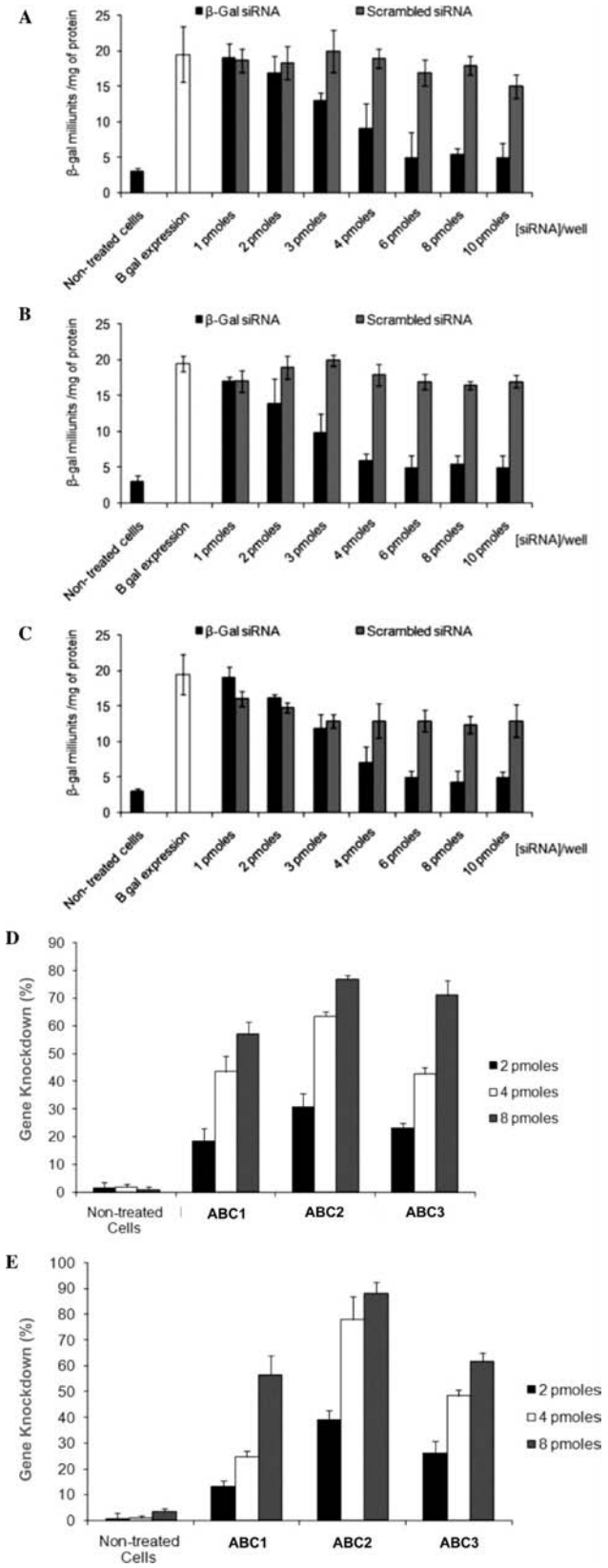

Figure 6. GAPDH gene knockdown in HepG2 cells following treatment with (A) 1 mol % **ABC1**, (B) 1 mol % **ABC2**, or (C) 1 mol % **ABC3** nanoparticles, all prepared at the lipid/siRNA charge ratio of 4 and added to cells to mediate exogeneous β-gal gene knockdown. All β-gal levels in HepG2 cells are expressed as β-gal milliunits/mg of protein. Data represent means of three separate experiments ± standard deviation. Similar results were obtained with HeLa and

dx.doi.org/10.1021/bc3004099 | *Bioconjugate Chem.* 2013, 24, 314−332

Figure 6. continued

HuH7 cell lines. GAPDH knockdown assay in Huh7 (D) and HepG2 (E) cells following treatment of cells with 1 mol % **ABC1**, 1 mol % **ABC2**, or 1 mol % **ABC3** nanoparticles formulated with anti-GAPDH siRNA or control at a lipid/siRNA charge ratio of 4. Differential effects of siRNA on endogeneous GAPDH protein levels analyzed with increasing concentrations of siRNA 2, 4, and 8 pmol/well. The data is average of 3 separate experiments ± SD.

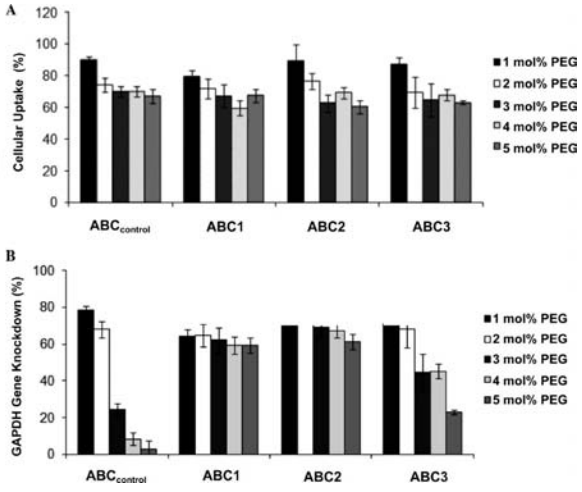

Figure 7. Effect of PEGylation on cellular uptake and gene knockdown mediated by **ABC** nanoparticles. (A) Percentage of HepG2 cellular uptake of FAM labeled siRNA formulated into $\mathbf{ABC}_{control}$, **ABC1**, **ABC2**, or **ABC3** nanoparticles formulated with a lipid/siRNA charge ratio of 4 and with the indicated levels of surface postcoupled PEG. The cellular uptake was measured using FACS ([siRNA] 20 pmol/well). (B) GAPDH protein level knockdown levels in HepG2 cells post treatment of cells with **ABC1**, **ABC2**, or **ABC3** nanoparticles ([siRNA] 8 pmol/well) as in Figure 6E. GAPDH gene knockdown was determined using KDalertGAPDH assay kit.

HepG2 cells (Figure 7B). Overall, **ABC2** type nanoparticles appeared to be the most effective agents of siRNA-mediated knockdown of protein levels and so were chosen to be the focus of the in vivo studies described below. These data (Figure 7) also appear consistent with a beneficial operation of pH-triggerability in vitro to overcome the inhibitory effects of PEGylation on efficient intracellular trafficking of nanoparticles and also on the functional intracellular delivery of RNAi payload.

Effect of PEGylation on Nanoparticle Uptake Pathways. GAPDH knockdown studies were performed with HepG2 cells in the presence of cell-uptake inhibitors (Table 2) intended to block the main pathways of nanoparticle-mediated nucleic acid entry into cells and intracellular trafficking (Scheme 4). The effect of these inhibitors on nanoparticle-

Table 2. Pharmacological Drugs Used for the Inhibition of Cellular Endocytic Pathways

drug	pathway inhibited	concentration
Nocodazole	Cytoskeleton	10 μM
Genistein	Caveolae	200 μM
Chlorpromazine	Clathrin	56 μM
Amiloride	Macropinocytosis	10 μM
ZfFG	Membrane fusion	50 μM

Scheme 4. Different Cell Uptake Pathways Involved in Nanoparticle Uptake into Cells

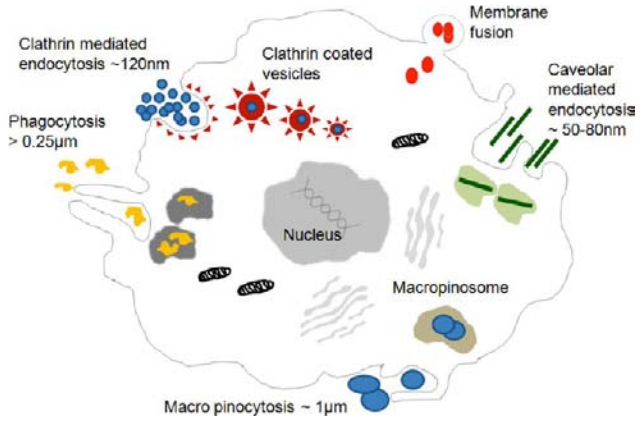

mediated siRNA delivery was studied using a series of **AB1**, **AB2**, and **AB3** lipoplex nanoparticles and corresponding 5 mol % **ABC1**, **ABC2**, and **ABC3** nanoparticles. Knockdown effects were evaluated once more with the KDalert GAPDH assay kit. Cellular uptake was assessed in parallel by FACS analysis (as above). Cellular uptake data (Figure 8A,B,C) clearly showed that cell entry of **AB1**, **AB2**, and **AB3** lipoplex nanoparticles was inhibited by ZfFG primarily that is associated with the inhibition of membrane fusion events. In the case of 5 mol % **ABC1**, **ABC2**, and **ABC3** nanoparticles, cellular uptake was inhibited by chlorpromazine primarily that traditionally inhibits clathrin-coated pit mediated uptake. Hence, PEGylated nanoparticles appear to enter cells by different entry mechanism to that of naked lipoplex nanoparticles (Figure 8A,B,C). In the case of specific GAPDH knockdown, 5 mol % **ABC1**, **ABC2**, or **ABC3** nanoparticle-mediated delivery was perturbed by chlorpromazine administration (as above), and also by ZfG administration, indicating that siRNA-mediated GAPDH knockdown by PEGylated siRNA-nanoparticles is dependent upon both clathrin-coated pit (for cell entry) and membrane fusion events (for functional, intracellular, siRNA delivery). By contrast, siRNA-mediated GAPDH knockdown by administration of **AB1**, **AB2**, and **AB3** lipoplex nanoparticles remained dependent on ZfFG administration alone and hence membrane fusion alone (Figure 8D,E,F).

Confocal microscopy experiments were performed on HepG2 cells using Alexa 488 fluorescent-labeled antitransferrin antibodies specific for clathrin-coated pit endosomes and Alexa 488 fluorescent-labeled anticholera toxin antibodies specific for caveolae. Consistent with inhibitor data, we observed that 5 mol % **ABC1**, **ABC2**, or **ABC3** nanoparticles labeled with DOPE-Rhoda were partially colocalized with antitransferrin antibodies (Figure 9A,B,C) but not at all with anticholera toxin antibodies (Figure 9D,E,F), consistent with the fact that the cellular entries of 5 mol % **ABC1**, **ABC2**, or **ABC3** nanoparticles appear to be closely associated with the clathrin-coated pit uptake mechanism. Nanoparticles appear to enter the cytoplasm of HepG2 cells in a similar manner to that seen previously,[29] with lipid and siRNA essentially colocalized, presumably in endosome/endosome-like compartments distributed throughout the cytoplasm but not in cell nuclei.

Functional Delivery of siRNA to Cells in Vivo—anti-HCV Therapy Proof of Concept. Initially, 5 mol % **ABC2** nanoparticles were prepared in 10% sucrose solution with 1

dx.doi.org/10.1021/bc3004099 | *Bioconjugate Chem.* 2013, 24, 314−332

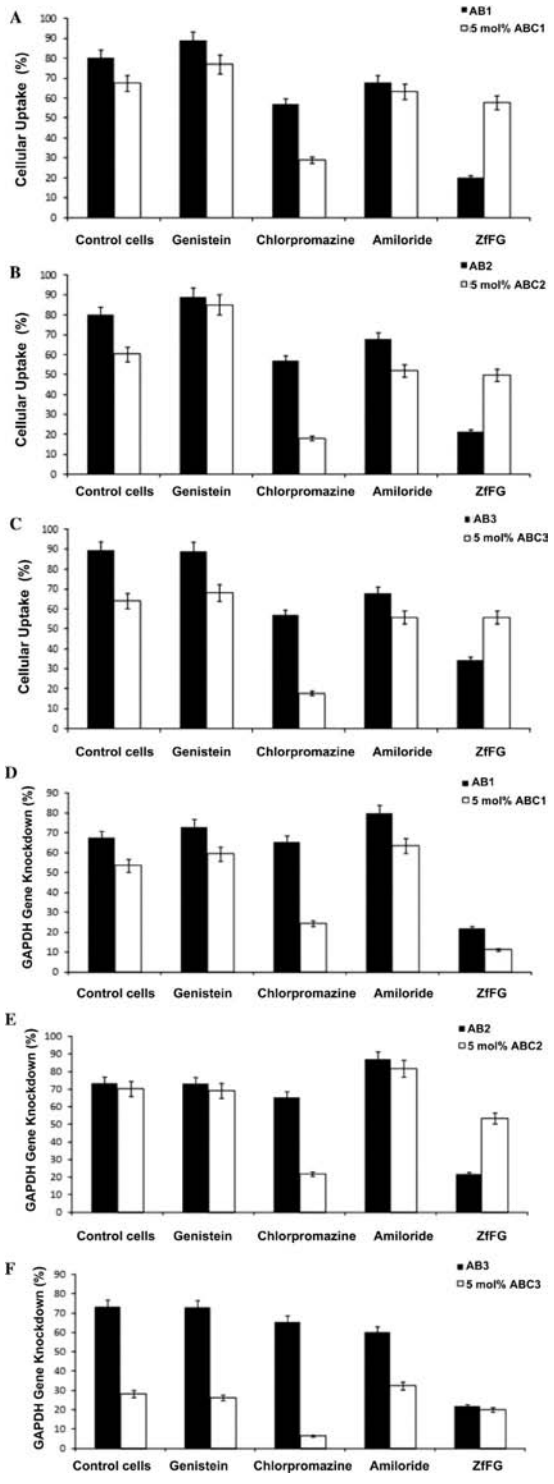

Figure 8. FACS analysis for percentage of HepG2 cell uptake of (A) **AB1** and 5 mol % **ABC1** nanoparticles, (B) **AB2** and 5 mol % **ABC2** nanoparticles, and (C) **AB3** and 5 mol % **ABC3** nanoparticles, formulated with lipid/siRNA charge ratio of 4, in the presence of inhibitors of cellular pathways ([siRNA] 20 pmol/well). The data are averages of 3 separate experiments ± SD. GAPDH gene knockdown in HepG2 cells mediated by (D) **AB1** and 5 mol % **ABC1** nanoparticles, (E) **AB2** and 5 mol % **ABC2** nanoparticles, and (F) **AB3** and 5 mol % **ABC3** nanoparticles, all formulated with lipid/siRNA charge ratio of 4 ([siRNA 8 pmol/well) in the presence of inhibitors of cellular uptake pathways. The percentage of GAPDH level reduction in cell lysate was determined using KDalert GAPDH kit. The data are averages of 3 separate experiments ± SD.

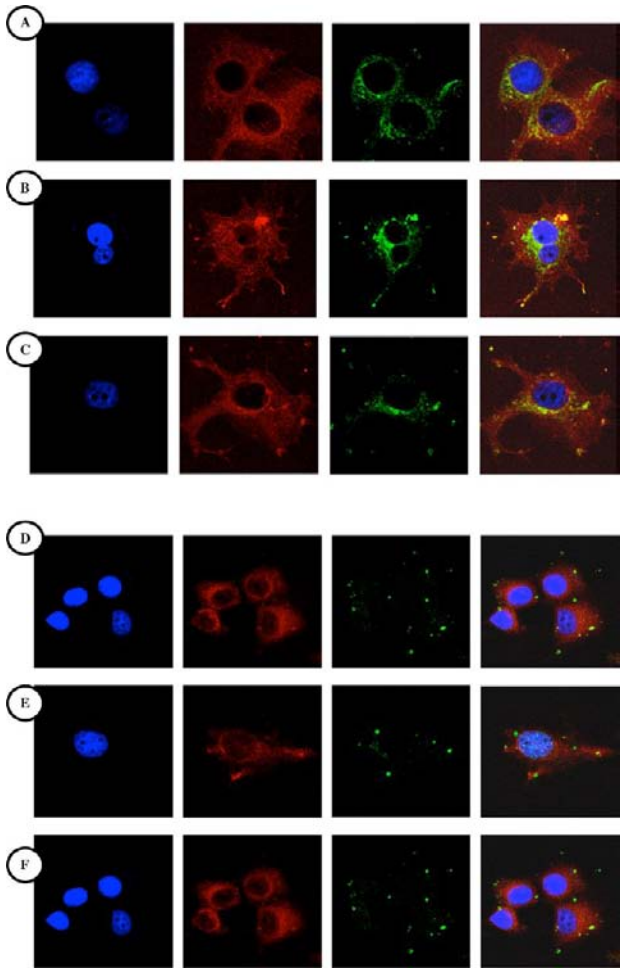

Figure 9. Intracellular location of Rhodamine labeled 5 mol % **ABC** nanoparticles ([siRNA] 100pmol/well), formulated with lipid/siRNA charge ratio of 4, in HepG2 cells using confocal microscopy. Rhodamine labeled nanoparticles colocalized with transferrin Alexa 488 after 1 h incubation, (A) 5 mol % **ABC1**, (B) 5 mol % **ABC2**, and (C) 5 mol % **ABC3**. Rhodamine labeled nanoparticles did not colocalize with cholera toxin B Alexa 488 after 1 h incubation, (D) 5 mol % **ABC1**, (E) 5 mol % **ABC2**, and (F) 5 mol % **ABC3** nanoparticles. Microscopic images were taken under the DAPI filter (first column), the Rhodamine filter (second column), and the Alexa-488 filter (third column). The images in the fourth column are an overlay of all three images.

mol % DOPE-Rhoda and Alexa 488 fluorescent-labeled siRNA (lipid/siRNA charge ratio 4). This nanoparticle system was introduced by intravenous (i.v.) administration (siRNA dose 3 mg/kg of animal body weight) in order to determine an in vivo biodistribution 24 h post administration (Figure 10A). At least 80% of the administered dose of siRNA was found in the liver. Liver histology and confocal microscopy revealed the colocalization of lipids and siRNA in at least 60% of hepatocytes in the visual field (Figure 10B).

Following this, 5 mol % **ABC2** nanoparticle-mediated siRNA-enabled gene knockdown was assessed in vivo using the following murine hydrodynamic injection (MHI) model. Murine livers (8 week old MF1 mice) were encouraged to uptake substantial amounts (5 μg/animal) of the nonintegrating, long-term expressing plasmid pLucA1 by hydrodynamic delivery. This plasmid is capable of expressing luciferase in liver hepatocytes for >6 months under control of the AAT liver

dx.doi.org/10.1021/bc3004099 | *Bioconjugate Chem.* 2013, 24, 314−332

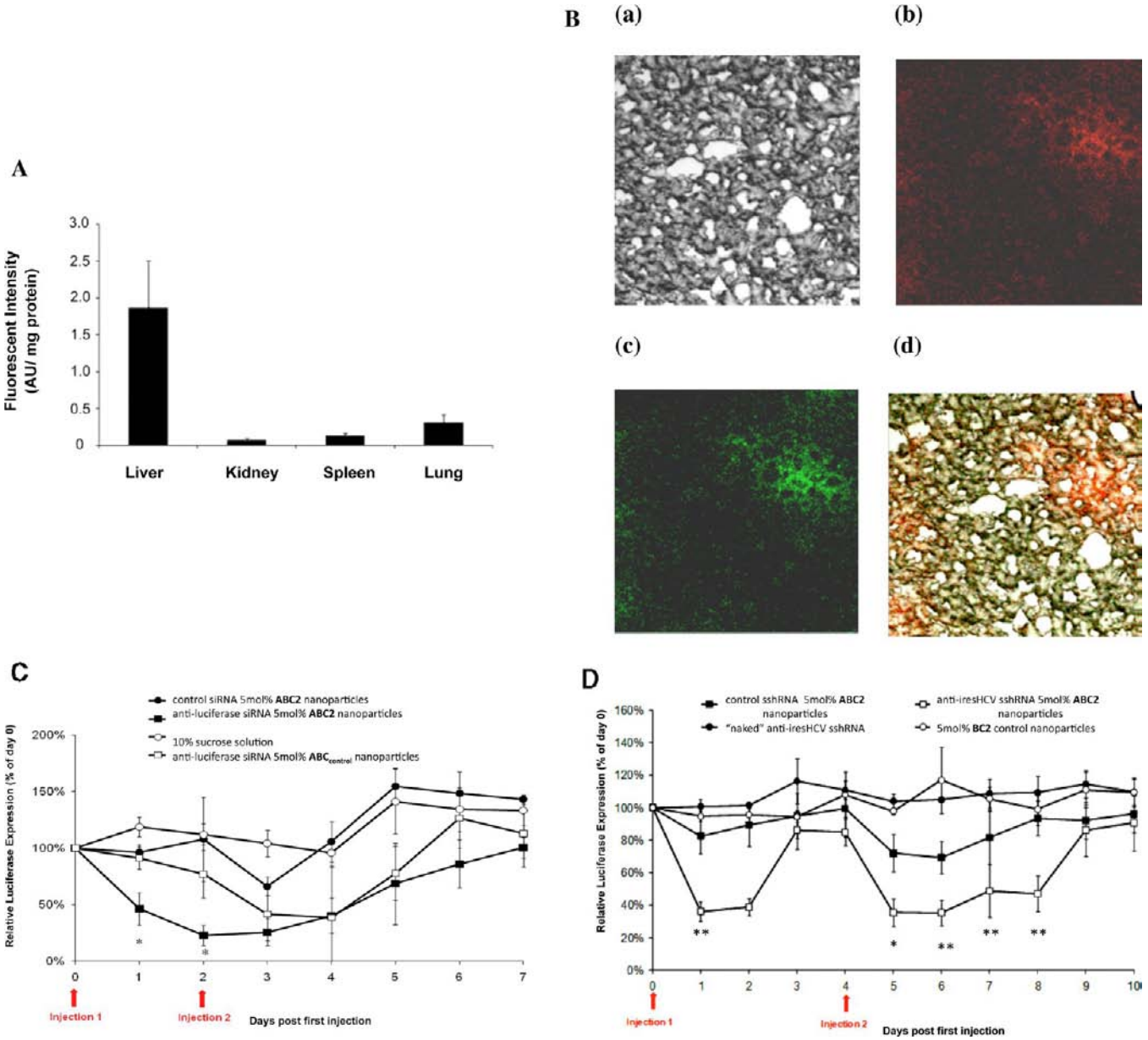

Figure 10. In vivo behavior of 5 mol % **ABC2** nanoparticles. (A) Tissue distribution of fluorescent labeled 5 mol % **ABC2** nanoparticles, formulated with lipid/siRNA charge ratio of 4 (siRNA dose, 3 mg/kg animal body weight), in liver, kidney, spleen, and lungs, harvested from MF1 mice 24 h post nanoparticle administration. The fluorescence intensity was normalized to the protein content using the BCA assay. The data are an average of measurements from the tissues harvested from 3 different animals ± SD. (B) Representative confocal microscopy images of mice liver containing Alexa-488 fluorescent-labeled siRNA and/or DOPE-Rhoda labeled nanoparticles; mice were treated by intravenous (i.v.) administration with 5 mol % **ABC2** nanoparticles (siRNA dose, 3 mg/kg animal body weight), formulated with lipid/siRNA charge ratio of 4, and livers were then harvested and sectioned for examination by confocal microscopy. Representative fields of view are (a) bright field image, (b) DOPE-Rhoda labeled nanoparticle image, (c) Alexa 488-labeled siRNA image, (d) overlaid image demonstrating colocalization of siRNA and nanoparticle lipids. (C) Luciferase expression from pLucA1 expressing in MHI-MF1 mice following treatment with 5 mol % **ABC2** nanoparticles delivering antiluciferase (■) or control siRNA (●). Other control treatments used in the experiments are 10% sucrose solution (○) and 5 mol % $\mathbf{ABC}_{\mathbf{control}}$ nanoparticles delivering antiluciferase siRNA (□) (each siRNA dose in all cases, 1 mg/kg animal body weight). The luciferase expression in livers of the different groups of animals was monitored for a week using Xenogen bioimaging. The data represent the relative luciferase expression normalized to the signal intensity measured before injecting nanoparticles (day 0) (percentage of day 0). The data represents the mean ± STD (n = 3). (D) Knockdown effects post administration of 5 mol % **ABC2** nanoparticles (lipid/RNAi effector charge ratio 4) on luciferase expression in HCV transgenic MHI-mice. MF1 mice received a pmarmTTRiresFLuc plasmid (5 μg/mouse). At 6 days post MHI, animals were injected (at the indicated times) with either anti-iresHCV sshRNA (□) or corresponding control sshRNA (■) (each RNAi effector dose 1 mg/kg of animal body weight). The effects of administering naked anti-iresHCV sshRNA (●) at the same effector dose, and 5 mol % BC2 cationic liposomes ("empty nanoparticle") (○) at the same corresponding lipid-equivalent dose were also assessed. Data are expressed as percentage of day 0 ± SEM. The difference between anti-iresHCV sshRNA or control sshRNA administration was found to be statistically significant (p = 0.006) (n = 6) and the difference between all controls was found to be statistically insignificant (p = 0.2) (n = 3).

dx.doi.org/10.1021/bc3004099 | *Bioconjugate Chem.* 2013, 24, 314−332

specific promoter without integration or traditional gene silencing.[24] Luciferase transgene expression in mice liver hepatocytes was then monitored by means of bioluminescence imaging (UVIS, Xenogen) for 6 days posthydrodynamic delivery of pLucA1. Expression was initially unstable but reduced to a state of stable passive maintenance by 6 days.[25]

At this point, 5 mol % **ABC2** nanoparticles were prepared in 10% sucrose solution with antiluciferase siRNA or a corresponding control siRNA. In addition, 5 mol % $\mathbf{ABC}_{\mathbf{control}}$ nanoparticles were also prepared (without oxime linkages by a premodification approach) using DODAG/Chol/DOPE/CPA (at 20:10:45:20 m/m/m/m) cationic liposomes, 5 mol % MeO-PEG^{2000}-DSPE, and the same antiluciferase siRNA or corresponding control siRNA. Nanoparticles were then administered twice at day 0 and day 2 (each siRNA dose 1 mg/kg of animal body weight) to luciferase transgene expressing mice. Bioluminescence changes were then monitored as a function of time (Figure 10C). Data demonstrate that administration of 5 mol % **ABC2** nanoparticles resulted in more rapid and more sustained luciferase knockdown effects than administration of 5 mol % $\mathbf{ABC}_{\mathbf{control}}$ nanoparticles. Hence these data (Figure 10C) suggest that the pH-trigger mechanism is operating in vivo (as in vitro, Figure 7) to overcome the inhibitory effects (at least in part) of PEGylation on efficient intracellular trafficking of nanoparticles and also on the functional intracellular delivery of RNAi payload.

Finally, the luciferase transgene experiment was followed by a proof of concept anti-HCV experiment. In this experiment, the anti-HCV RNAi effectors selected were anti-iresHCV specific and control sshRNA sequences developed and provided by Somagenics Inc. (Santa Cruz, CA, USA).[26,27] The ires target sequence is the most conserved region of an otherwise rapidly mutating HCV genome sequence, and therefore represents a logical target within the HCV genome. For our proof of concept experiment, a variant of the MHI model was created using the alternative luciferase (FLuc) gene expressing plasmid pmarmTTRiresFLuc (Somagenics Inc.) that comprised a luciferase gene rendered chimeric by in frame fusion with the HCV ires sequence. The guiding principle behind this experiment was that successful RNAi-mediated knockdown of the chimeric gene through ires sequence targeting would bring about a concomitant down-regulation of expressed luciferase levels in the murine hepatocytes as above, that could be monitored once again as a function of time by means of bioluminescence imaging (UVIS, Xenogen).

As before, murine livers (8 week old MF1 mice) were encouraged to uptake substantial amounts (5 μg/animal) of pmarmTTRiresFLuc plasmid by hydrodynamic delivery, then luciferase transgene expression was monitored once again by bioluminescence imaging in mice liver hepatocytes for 6 days posthydrodynamic delivery. Thereafter, 5 mol % **ABC2** nanoparticles were prepared in 10% sucrose solution with anti-ires sshRNA or a corresponding control sshRNA. Additional controls used were naked antiluciferase sshRNA and an "empty nanoparticle" control, namely, a PEGylated cationic liposome (5 mol % **BC2** cationic liposomes) without sshRNA in association. Nanoparticles were then administered twice at day 0 and day 4 (each sshRNA dose 1 mg/kg of animal body weight where appropriate) to MHI luciferase transgene-expressing model mice. Subsequent changes in bioluminescence were monitored as a function of time as previously (Figure 10D). Administration of 5 mol % **ABC2** nanoparticles prepared with sshRNA was clearly demonstrated to result in specific, functional RNAi mediated luciferase knockdown effects over 2 days post the day 0 administration and 4 days post day 4 of administration. On the other hand, there was some evidence for nonspecific RNAi mediated knockdown effects following day 2 administration of the control sshRNA, consistent with the possible overloading in vivo of murine hepatocytes with RNAi effector.

Accordingly, experiments were performed with each administered sshRNA dose reduced to 0.3 mg/kg of animal body weight. Compared with the first experiment, similar levels of luciferase knockdown (>70% relative to controls) were observed but only after two consecutive administrations (day 0 and day 2) of 5 mol % **ABC2** nanoparticles with antiluciferase sshRNA, as opposed to just a single day 0 administration at 1 mg/kg (data not shown). These data do suggest that changes in dose and time should be useful parameters for future investigation in order to optimize knockdown durability and efficiency. Throughout all studies reported above, we observed no adverse reactions with any one of the experimental groups that would be consistent with nanoparticle-induced in vivo toxicity, although extensive preclinical toxicology studies will be essential to include going forward.

DISCUSSION

The data described here represent the completion of a systematic study of PEGylated siRNA-nanoparticles based upon our original siFECTplus nanoparticle system reported previously. Our intention in carrying out this study was to test and reinforce principles outlined in our previous publication on this subject.[14] Three cationic liposome formulations are described **CL1**, **CL2**, and **CL3** prepared (Table 1) from which different lipoplex nanoparticles **AB1**, **AB2**, and **AB3** were prepared, respectively. **AB2** lipoplex nanoparticles with a lipid/siRNA charge ratio of 4 (that corresponds with a 12:1 w/w lipid/siRNA ratio) were the most favorable lipoplex nanoparticles in vitro, and appeared to offer the best combination of efficacy with minimal toxicity and minimal overall charge (ζ-potential) (Figures 2 and 3; see Supporting Information Figures S1 and S2). These nanoparticles make primary use of our most recently reported cationic lipid DODAG **1** and the neutral colipid DOPE **2** (Figure 1).[13] Following on from this, 1 mol % **ABC2** (PEGylated) nanoparticles were shown to mediate optimal β-gal and GAPDH knockdown in vitro using HeLa, HepG2, and Huh7 cells, but were not colloidally stable in serum (Figure 6; see Supporting Information Figure S3). In contrast, 5 mol % **ABC2** nanoparticles were colloidally stable in serum and were also able to mediate GAPDH knockdown in HepG2 cells in vitro (Figures 4 and 7). Accordingly, 5 mol % **ABC2** nanoparticles were used to mediate functional delivery of RNAi effectors in vivo including the delivery of an anti-iresHCV sshRNA construct to mice livers in a MHI model of HCV infection developed for our purposes here (Figure 10D).

Critically, our data support the inclusion of pH-triggerability into our nanoparticle design for functional delivery of RNAi effectors by PEGylated nanoparticles in vitro and in vivo. Evidence for the capacity of the 5 mol % **ABC1**, **ABC2**, and **ABC3** nanoparticles for pH-triggered release of siRNA under mildly acidic conditions was provided by incubation and gel retardation assays (Figure 5). In mechanistic terms, these observed pH stability profiles deserve some explanation. Formation of **ABC1**, **ABC2**, and **ABC3** nanoparticles takes place at pH 4 that is known in physical organic chemistry circles to be an optimal pH for oxime formation from the combination

dx.doi.org/10.1021/bc3004099 | Bioconjugate Chem. 2013, 24, 314−332

of an aminoxy functional group and an aldehyde (see Scheme 3). At this pH, the reaction is committed and oxime product once formed does not reverse to reactants. Oximes once formed are stable at pH 7 but are increasingly subject to general acid-catalyzed hydrolytic decomposition as environmental pH is lowered until the pH is sufficiently low for oxime formation to be substantially promoted over hydrolytic decomposition once more. Oxime decomposition under mildly acidic conditions might contribute to pH-triggered release of entrapped siRNA, but we would suggest that such decomposition must act in synergy with other nanoparticle structural changes yet to be characterized and understood in order to promote the dramatic observed effects of pH on siRNA release (Figure 5).

In vitro evidence appears to suggest that the property of pH-triggerability assists nanoparticles with higher levels of surface PEGylation (>2 mol %) to achieve functional delivery of siRNA in contrast to the situation with corresponding control pH-stable PEGylated nanoparticles (Figure 7). We would suggest that this is a consequence of the cellular uptake mechanism of nanoparticles. Uptake inhibitor data showed that lipoplex nanoparticles enter HepG2 cells and mediate functional delivery of siRNA by mechanism(s) that rely on membrane fusion, whereas PEGylated nanoparticles appear to enable functional delivery of siRNA by mechanism(s) that rely on clathrin-coated pit endocytosis (for cellular uptake) and membrane fusion events (for functional intracellular RNAi effector delivery) (Figure 8). The internal vacuoles of endosome vesicles are known to acidify (pH 7 to 5.8) in time periods of up to 6 h post endocytosis in preparation for lysozomal fusion.[30] Therefore, our current hypothesis for the mechanism of RNAi effector delivery by our pH-triggered PEGylated siRNA-nanoparticles is as follows. Once nanoparticles have entered cells by endocytosis at pH 7, they begin to lose stability as pH drops and a partial release of PEG surface coverage takes place due to oxime hydrolysis. This latter process then leads to the formation of "exposed lipid patches" at nanoparticle surfaces thereby setting up possibilities for endosomolysis mediated by fusogenic events between nanoparticle and endosome membranes. The release of RNAi effector into cell cytosols then follows.

Overall, our pH-triggered PEGylated siRNA-nanoparticles would appear to have characteristics compatible with and suitable for controlled release of RNAi effectors in cellular endosome compartments thereby allowing for the possibility of enhanced functional release of siRNA into cellular cytoplasm in conjunction with subsequent endosomolysis. In the absence of pH-triggerability, PEGylated nanoparticles are much less able to release siRNA from nanoparticle association and hence less able to achieve functional delivery of siRNA (Figures 7 and 10). We would ascribe this impaired release (in large part) to the steric blocking effect of a largely intact PEG stealth/biocompatibility polymer layer postcellular entry.[31]

While all these data are encouraging, there is room for improvement in nanoparticle design. The in vivo delivery data certainly demonstrate proof of concept for HCV therapy mediated by an RNAi effector. However, repeat doses of the sshRNAi inhibitor were only able to mediate a 2−3-fold downregulation in the levels of the luciferase protein in liver, when we really require a 100-fold drop in protein levels at least over several weeks for therapy to be realizable. On the other hand, preliminary data do suggest that a well-designed dose regime could have more pronounced effects. Nevertheless although we are seeing opportunities for RNAi-mediated effects using RNAi effector doses of 1 mg/kg of animal body weight or less, such doses themselves are also too high by at least 100-fold for routine therapy. Consequently, proof of HCV therapy should really be accomplished at a level 10^4-fold more effective than currently appears possible. How can we get there? Recent knockdown data obtained using lipid and lipidoid-based nanoparticle delivery vectors suggest that careful alterations to the chemical structure of key components of RNAi delivery vector systems can increase the potency of RNAi effects.[11,12] In addition, chemical modification of RNAi effectors and different RNAi effectors can also promote potency and prolong the duration of RNAi-mediated gene knockdown effects and downregulation of associated protein levels.[32,33] Finally, an increased understanding of RNAi effector intracellular trafficking are certain to provide additional, important information to minimize off-target effects and maximize the efficiency of delivery.[34−36] Accordingly, there remain substantial opportunities for further development toward lipid-based nanoparticle delivery systems suitable for routine clinical use.

CONCLUSIONS

The 5 mol % **ABC2** nanoparticles are a sound platform from which to construct in vivo siRNA-therapeutic approaches for the treatment of liver disorders and other diseases.

ASSOCIATED CONTENT

Supporting Information

In vitro FACS experiments and in vitro toxicology data referred to in the main text. This material is available free of charge via the Internet at http://pubs.acs.org.

AUTHOR INFORMATION

Corresponding Author

*E-mail: a.miller07@btinternet.com.

Notes

The authors declare the following competing financial interest(s): Brian Johnston (author) is an officer of the collaborating company Somagenics named on this manuscript.

ACKNOWLEDGMENTS

We thank the Mitsubishi Chemical Corporation, IC-Vec Ltd, and Somagenics for the provision of financial support for the Imperial College Genetic Therapies Centre.

ABBREVIATIONS

siRNA, small interfering RNA; RNAi, RNA interference; pDNA, plasmid DNA; HBV, hepatitis B virus; HCV, hepatitis C virus; DODAG, *N*′,*N*′-dioctadecyl-*N*-4,8-diaza-10-aminodecanoylglycylamide; CDAN, N^1-cholesteryloxycarbonyl-3,7-diazanonane-1,9-diamine; DOPE, dioleoyl-L-α-phosphatidylethanolamine; DOPC, dioleoyl-L-α-phosphatidylcholine; Chol, cholesterol; CPA, cholesteryl PEG^{350}-aminoxy lipid; PEG, polyethylene glycol; PEG^{2000}-$(CHO)_2$, polyethylene glycol 2000-dialdehyde; PCS, photon correlation spectroscopy; DMEM, Dulbecco's Modified Eagle's Medium; EDTA, ethylenediamine tetraacetic acid; TE, Tris-HCl/EDTA buffer; TBE, Tris-Borate/EDTA buffer; HEPES, 2-[4-(2-hydroxyethyl)-piperazin-1-yl]ethanesulfonic acid; DMAP, dimethylaminopyridine; HBTU, 2-(1*H*-benzotriazole-1-yl)-1,1,3,3-tetramethyluronium hexafluorophosphate; BCA, bicinchoninic acid; FACS, fluorescence-activated cell sorting; PBS, phosphate-

buffered saline; ZfFG, carbobenzoxy-D-phenylalanine-L-phenylalanine-glycine; DOPE-Rhoda, dioleoyl-L-α-phosphatidyl-ethanolamine-*N*-(lissamine rhodamine B sulfonyl); FCS, bovine or fetal calf serum; GAPDH, glyceraldehyde-3-phosphate dehydrogenase; OCT, optimal cutting temperature; PFA, paraformaldehyde; MHI, murine hydrodynamic injection; MeO-PEG^{2000}-DSPE, (ω-methoxy-polyethylene glycol 2000)-*N*-carboxy-distearoyl-L-α-phosphatidylethanolamine; sshRNA, short stem, small hairpin RNA; ires, internal ribosome entry site; LDH assay, lactate dehydrogenase assay; ddH_2O, double distilled H_2O; β-gal, β-galactosidase

REFERENCES

(1) Dykxhoorn, D. M. (2009) RNA interference as an anticancer therapy: a patent perspective. *Expert Opin. Ther. Pat. 19*, 475−491.

(2) Dykxhoorn, D. M., and Lieberman, J. (2006) Knocking down disease with siRNAs. *Cell 126*, 231−235.

(3) Dykxhoorn, D. M., Palliser, D., and Lieberman, J. (2006) The silent treatment: siRNAs as small molecule drugs. *Gene Ther. 13*, 541−552.

(4) Juliano, R. L. (2005) Peptide-oligonucleotide conjugates for the delivery of antisense and siRNA. *Curr. Opin. Mol. Ther. 7*, 132−136.

(5) Ikeda, Y., and Taira, K. (2006) Ligand-targeted delivery of therapeutic siRNA. *Pharm. Res. 23*, 1631−1640.

(6) Aigner, A. (2006) Gene silencing through RNA interference (RNAi) in vivo: strategies based on the direct application of siRNAs. *J. Biotechnol. 124*, 12−25.

(7) Jere, D., Jiang, H. L., Arote, R., Kim, Y. K., Choi, Y. J., Cho, M. H., Akaike, T., and Cho, C. S. (2009) Degradable polyethylenimines as DNA and small interfering RNA carriers. *Expert Opin. Drug Delivery 6*, 827−834.

(8) Honma, K., Miyata, T., and Ochiya, T. (2004) The role of atelocollagen-based cell transfection array in high-throughput screening of gene functions and in drug discovery. *Curr. Drug Discovery Technol. 1*, 287−294.

(9) Gao, K., and Huang, L. (2009) Nonviral methods for siRNA delivery. *Mol. Pharmaceutics 6*, 651−658.

(10) Tseng, Y. C., Mozumdar, S., and Huang, L. (2009) Lipid-based systemic delivery of siRNA. *Adv. Drug Delivery Rev. 61*, 721−731.

(11) Semple, S. C., Akinc, A., Chen, J., Sandhu, A. P., Mui, B. L., Cho, C. K., Sah, D. W., Stebbing, D., Crosley, E. J., Yaworski, E., Hafez, I. M., Dorkin, J. R., Qin, J., Lam, K., Rajeev, K. G., Wong, K. F., Jeffs, L. B., Nechev, L., Eisenhardt, M. L., Jayaraman, M., Kazem, M., Maier, M. A., Srinivasulu, M., Weinstein, M. J., Chen, Q., Alvarez, R., Barros, S. A., De, S., Klimuk, S. K., Borland, T., Kosovrasti, V., Cantley, W. L., Tam, Y. K., Manoharan, M., Ciufolini, M. A., Tracy, M. A., de Fougerolles, A., MacLachlan, I., Cullis, P. R., Madden, T. D., and Hope, M. J. (2010) Rational design of cationic lipids for siRNA delivery. *Nat. Biotechnol. 28*, 172−176.

(12) Love, K. T., Mahon, K. P., Levins, C. G., Whitehead, K. A., Querbes, W., Dorkin, J. R., Qin, J., Cantley, W., Qin, L. L., Racie, T., Frank-Kamenetsky, M., Yip, K. N., Alvarez, R., Sah, D. W., de Fougerolles, A., Fitzgerald, K., Koteliansky, V., Akinc, A., Langer, R., and Anderson, D. G. (2010) Lipid-like materials for low-dose, in vivo gene silencing. *Proc. Natl. Acad. Sci. U.S.A. 107*, 1864−1869.

(13) Mével, M., Kamaly, N., Carmona, S., Oliver, M. H., Jorgensen, M. R., Crowther, C., Salazar, F. H., Marion, P. L., Fujino, M., Natori, Y., Thanou, M., Arbuthnot, P., Yaouanc, J.-J., Jaffres, P. A., and Miller, A. D. (2010) DODAG; a versatile new cationic lipid that mediates efficient delivery of pDNA and siRNA. *J. Controlled Release 143*, 222−232.

(14) Carmona, S., Jorgensen, M. R., Kolli, S., Crowther, C., Salazar, F. H., Marion, P. L., Fujino, M., Natori, Y., Thanou, M., Arbuthnot, P., and Miller, A. D. (2009) Controlling HBV replication in vivo by intravenous administration of triggered PEGylated siRNA-nanoparticles. *Mol. Pharmaceutics 6*, 706−717.

(15) Kenny, G. D., Kamaly, N., Kalber, T. L., Brody, L. P., Sahuri, M., Shamsaei, E., Miller, A. D., and Bell, J. D. (2011) Novel multifunctional nanoparticle mediates siRNA tumour delivery, visualisation and therapeutic tumour reduction *in vivo*. *J. Controlled Release 149*, 111−116.

(16) Kostarelos, K., and Miller, A. D. (2005) Synthetic, self-assembly ABCD nanoparticles; a structural paradigm for viable synthetic non-viral vectors. *Chem. Soc. Rev. 34*, 970−994.

(17) Huang, L., and Liu, Y. (2011) *In vivo* delivery of RNAi with lipid-based nanoparticles. *Annu. Rev. Biomed. Eng. 13*, 507−530.

(18) Aissaoui, A., Chami, M., Hussein, M., and Miller, A. D. (2011) Efficient topical delivery of plasmid DNA to lung in vivo mediated by putative triggered, PEGylated pDNA nanoparticles. *J. Controlled Release 154*, 275−284.

(19) Drake, C. R., Aissaoui, A., Argyros, O., Serginson, J. M., Monnery, B. D., Thanou, M., Steinke, J. H. G., and Miller, A. D. (2010) Bioresponsive small molecule polyamines as non-cytotoxic alternative to polyethylenimine. *Mol. Pharmaceutics 7*, 2040−2055.

(20) Cooper, R. G., Etheridge, C. J., Stewart, L., Marshall, J., Rudginsky, S., Cheng, S. H., and Miller, A. D. (1998) Polyamine analogues of 3β-[*N*-(*N*′,*N*′-dimethylaminoethane)carbamoyl]-cholesterol (DC-Chol) as agents for gene delivery. *Chem. Eur. J. 4*, 137−152.

(21) Keller, M., Jorgensen, M. R., Perouzel, E., and Miller, A. D. (2003) Thermodynamic aspects and biological profile of CDAN/DOPE and DC-Chol/DOPE lipoplexes. *Biochemistry 42*, 6067−6077.

(22) Oliver, M., Jorgensen, M. R., and Miller, A. D. (2004) The facile solid-phase synthesis of cholesterol-based polyamine lipids. *Tetrahedron Lett. 45*, 3105−3108.

(23) Still, W. C., Kahn, M., and Mitra, A. (1978) Rapid chromatographic techniques for preparative separation with moderate resolution. *J. Org. Chem. 43*, 2923−2925.

(24) Argyros, O., Wong, S. P., Niceta, M., Waddington, S. N., Howe, S. J., Coutelle, C., Miller, A. D., and Harbottle, R. P. (2008) Persistent episomal transgene expression in liver following delivery of a scaffold/matrix attachment region containing non-viral vector. *Gene Ther. 15*, 1593−1605.

(25) Morrissey, D. V., Lockridge, J. A., Shaw, L., Blanchard, K., Jensen, K., Breen, W., Hartsough, K., Machemer, L., Radka, S., Jadhav, V., Vaish, N., Zinnen, S., Vargeese, C., Bowman, K., Shaffer, C. S., Jeffs, L. B., Judge, A., MacLachlan, I., and Polisky, B. (2005) Potent and persistent in vivo anti-HBV activity of chemically modified siRNAs. *Nat. Biotechnol. 23*, 1002−1007.

(26) Ge, Q., Dallas, A., Ilves, H., Shorenstein, J., Behlke, M. A., and Johnston, B. H. (2010) Effects of chemical modification on the potency, serum stability, and immunostimulatory properties of short shRNAs. *RNA 16*, 118−130.

(27) Ge, Q., Ilves, H., Dallas, A., Kumar, P., Shorenstein, J., Kazakov, S. A., and Johnston, B. H. (2010) Minimal-length short hairpin RNAs: the relationship of structure and RNAi activity. *RNA 16*, 106−117.

(28) Stewart, L., Manvell, M., Hillery, E., Etheridge, C. J., Cooper, R. G., Stark, H., van-Heel, M., Preuss, M., Alton, E. W. F. W., and Miller, A. D. (2001) Physico-chemical analysis of cationic liposome-DNA complexes (lipoplexes) with respect to in vitro and in vivo gene delivery efficiency. *J. Chem. Soc., Perkin Trans. 2*, 624−632.

(29) Spagnou, S., Miller, A. D., and Keller, M. (2004) Lipidic carriers of siRNA: differences in the formulation, cellular uptake, and delivery with plasmid DNA. *Biochemistry 43*, 13348−13356.

(30) Serresi, M., Bizzarri, R., Cardarelli, F., and Beltram, F. (2009) Real-time measurement of endosomal acidification by a novel genetically encoded biosensor. *Anal. Bioanal. Chem. 393*, 1123−1133.

(31) Keller, M., Harbottle, R. P., Perouzel, E., Colin, M., Shah, I., Rahim, A., Vaysse, L., Bergau, A., Moritz, S., Brahimi-Horn, C., Coutelle, C., and Miller, A. D. (2003) Nuclear localisation sequence templated nonviral gene delivery vectors: investigation of intracellular trafficking events of LMD and LD vector systems. *ChemBioChem 4*, 286−298.

(32) Zhou, J., Neff, C. P., Liu, X., Zhang, J., Li, H., Smith, D. D., Swiderski, P., Aboellail, T., Huang, Y., Du, Q., Liang, Z., Peng, L., Akkina, R., and Rossi, J. J. (2011) Systemic administration of

combinatorial dsiRNAs via nanoparticles efficiently suppresses HIV-1 infection in humanized mice. *Mol. Ther. 19*, 2228−2238.
(33) Zimmermann, T. S., Lee, A. C., Akinc, A., Bramlage, B., Bumcrot, D., Fedoruk, M. N., Harborth, J., Heyes, J. A., Jeffs, L. B., John, M., Judge, A. D., Lam, K., McClintock, K., Nechev, L. V., Palmer, L. R., Racie, T., Rohl, I., Seiffert, S., Shanmugam, S., Sood, V., Soutschek, J., Toudjarska, I., Wheat, A. J., Yaworski, E., Zedalis, W., Koteliansky, V., Manoharan, M., Vornlocher, H. P., and MacLachlan, I. (2006) RNAi-mediated gene silencing in non-human primates. *Nature 441*, 111−114.
(34) Detzer, A., Overhoff, M., Wunsche, W., Rompf, M., Turner, J. J., Ivanova, G. D., Gait, M. J., and Sczakiel, G. (2009) Increased RNAi is related to intracellular release of siRNA via a covalently attached signal peptide. *RNA 15*, 627−636.
(35) Mescalchin, A., Detzer, A., Wecke, M., Overhoff, M., Wunsche, W., and Sczakiel, G. (2007) Cellular uptake and intracellular release are major obstacles to the therapeutic application of siRNA: novel options by phosphorothioate-stimulated delivery. *Expert Opin. Biol. Ther. 7*, 1531−1538.
(36) Basha, G., Novobrantseva, T. I., Rosin, N., Tam, Y. Y., Hafez, I. M., Wong, M. K., Sugo, T., Ruda, V. M., Qin, J., Klebanov, B., Ciufolini, M., Akinc, A., Tam, Y. K., Hope, M. J., and Cullis, P. R. (2011) Influence of cationic lipid composition on gene silencing properties of lipid nanoparticle formulations of siRNA in antigen-presenting cells. *Mol. Ther. 19*, 2186−2200.